POLYMER ENGINEERING AND SCIENCE

Research Article

Rheological, mechanical and life cycle assessment of 3D-printed PLA/Hemp/PEG biocomposites

Submission ID ce6ceb49-07fd-4f00-a6b5-4add8ea41d5c

Submission Version Revision 1

PDF Generation 09 Feb 2026 01:22:12 EST by Atypon ReX

Authors

Faleh Rabhi
Corresponding Author
Submitting Author

ORCiD
https://orcid.org/0009-0002-5016-4460

CRediT
Conceptualization, Writing - original draft, Investigation, Methodology

Affiliations
- Université Marie et Louis Pasteur, CNRS, Institut FEMTO-ST, Besançon, F-25000, France

Ndeye Fatim Niang

CRediT
Investigation, Conceptualization

Affiliations
- Université Marie et Louis Pasteur, CNRS, Institut FEMTO-ST, Besançon, F-25000, France

Liam Cloëz

CRediT
Investigation

Affiliations
- Université Marie et Louis Pasteur, CNRS, Institut FEMTO-ST, Besançon, F-25000, France

Thierry Barriere

CRediT
Supervision, Validation

Affiliations
- Université Marie et Louis Pasteur, CNRS, Institut FEMTO-ST, Besançon, F-25000, France

Mehdi Belhani

CRediT
Investigation, Methodology

Affiliations
- National Higher School of Technology and Engineering, L3M, 23005, Annaba, Algeria

Mohamed Sahli

CRediT
Validation, Supervision

Affiliations

- Centre de recherche sur les Ions, les Matériaux et la Photonique, Université Caen Normandie, ENSICAEN, CNRS, CEA, Normandie Univ, CIMAP UMR6252, F-14000 CAEN

Additional Information

Research Topics

Yes

Research Topics

biopolymers; additive manufacturing; rheology; mechanical properties; composites

Files for peer review

All files submitted by the author for peer review are listed below. Files that could not be converted to PDF are indicated; reviewers are able to access them online.

Name	Type of File	Size	Page
Article PES - final version.docx	Main Document - MS Word	2.5 MB	Page 4
Article PES - corrections.docx	Main Document - Tracked Changes	2.8 MB	Page 36
Cover letter.docx	Author Response	25.2 KB	Page 70
graphical_abstract.jpg	Graphical Abstract Image	115.5 KB	Page 74

Rheological, mechanical and life cycle assessment of 3D-printed PLA/Hemp/PEG biocomposites

Faleh Rabhi [a*], Ndeye Fatim Niang [a], Liam Cloëz [a], Thierry Barriere [a], Mehdi Belhani [b], Mohamed Sahli [c]

[a] Université Marie et Louis Pasteur, CNRS, Institut FEMTO-ST, Besançon, F-25000, France

[b] National Higher School of Technology and Engineering, L3M, 23005, Annaba, Algeria

[c] Centre de recherche sur les Ions, les Matériaux et la Photonique, Université Caen Normandie, ENSICAEN, CNRS, CEA, Normandie Univ, CIMAP UMR6252, F-14000 CAEN

***Corresponding author**

Email address: faleh.rabhi@femto-st.fr

Abstract

There is considerable interest in the development of bio-based materials for pellet-based material extrusion 3D printing as sustainable alternatives to conventional polymer composites. This study investigates Poly(Lactic Acid) (PLA) biocomposites reinforced with 20 wt% short Hemp fibers and modified with 5 wt% Polyethylene Glycol (PEG) as an additive. The rheological behavior of the biocomposite melts was analyzed using the Carreau–Yasuda model at different temperatures. Chemical behavior was evaluated through rheological tests coupled with fast-scan Fourier transform infrared (FTIR) spectroscopy conducted at 190 °C, 200 °C, and 210 °C. A design of experiments approach was employed to optimize the 3D printing parameters and to assess the influence of extrusion temperature, printing speed, and layer thickness on print quality. The optimal printing conditions for Hemp-based parts were identified as a temperature of 200 °C, a printing speed of 35 mm/s, and 0.5 mm of layer thickness. Mechanical testing was performed to evaluate the effect of Hemp fiber reinforcement on the performance of PLA-based printed parts, revealing a significant influence of Hemp fibers on the mechanical properties. In addition, a Life Cycle Assessment (LCA) was conducted to quantify the environmental impact of the PLA/Hemp/PEG. The results demonstrate that these materials represent a promising eco-friendly solution for sustainable additive manufacturing applications.

Highlights:

- Sustainable bio-based pellet-extrusion 3D printing is demonstrated
- Processing temperature effects on rheology and chemistry are analyzed
- Optimal printing conditions are 200 °C, 35 mm/s, and 0.5 mm layer thickness
- Hemp fibers significantly affect PLA mechanical properties
- LCA confirms the environmental benefits of PLA/Hemp/PEG composites.

Keywords: Biocomposite, Biopolymer, Natural Fiber, Rheology, Mechanical Properties, Additive Manufacturing.

Nomenclature

T_m	Melting temperature (°C)
a	Transition factor
n	Pseudo plasticity index
Pc	Porosity (%)
P_{wt}	Printed weight (kg)
T	Temperature (°C)
T_{wt}	Theoretical weight (kg)
V	Volume (m^3)
η_0	Zero-shear rate viscosity (Pa s)
η_∞	Infinite shear viscosity (Pa s)
λ	Characteristic time (s)
$\bar{\dot{\gamma}}$	Generalized shear rate (s^{-1})
ρ	Density (kg m^{-3})

1. Introduction

Additive Manufacturing (AM) began to emerge in the 1980s with the development of stereolithography [1, 2], which introduced the concept of building components layer by layer [3, 4]. Since then, AM has significantly reshaped conventional manufacturing process. It is now regarded as a valuable complement to conventional production methods, particularly well-suited for single-part fabrication, small-batch production, and the manufacturing of components with complex geometries, such as lattice structures [5, 6]. Moreover, the environmentally friendly and sustainable characteristics of AM have been key drivers of its rapid growth, as industries increasingly seek to reduce material waste and energy consumption [7, 8]. In recent years, the scope of AM applications has expanded steadily, especially in the automotive, medical, and aerospace industries [9–12]. A typical AM process involves several critical steps [13], including part design, data conversion, file transfer, printing preparation, and the layer-by-layer fabrication of the component using AM equipment until completion. Today, 3D printing is transitioning from a prototyping tool to a method for producing end-use parts. According to the Wohler's Report 2023, the global 3D printing industry reached $18 billion in 2022, with an annual growth rate of 18.3%. Its adoption continues to deepen across aerospace (16%), healthcare (14%), and automotive (12%). Advances in materials—such as metals, ceramics, and composites—and improvements in printing speed are expected to further strengthen its advantages and promote greater digitalization and flexibility within the manufacturing sector [14, 15]. Among AM technologies, Fused Deposition Modeling (FDM) is one of the most widely used solid-based processes. It enables the fabrication of three-dimensional components through the layer-by-layer deposition of thermoplastic materials. FDM has become one of the most accessible and cost-effective AM techniques, commonly used for rapid prototyping, functional component production, and materials research. Its versatility, ease of use, and ability to produce durable parts make it a preferred choice in aerospace, automotive, medical, and educational fields [16, 17]. The FDM process operates by extruding a continuous filament of thermoplastic material through a heated nozzle, which deposits the material along a predetermined toolpath to create successive layers [18]. Among the materials frequently utilized in FDM, Poly(Lactic Acid) (PLA) is widely favored due to its biodegradability, printability, and minimal warping tendency. However, its low thermal resistance (approximately 60 °C) and relatively brittle mechanical properties limit its use in high-performance applications.

In recent years, natural fiber-reinforced polymer composites (NFRPCs) have gained considerable attention as sustainable alternatives to conventional FDM materials. Plant fibers exhibit a broad range of physical and mechanical properties that are strongly influenced by their chemical composition, microstructural organization, and botanical origin. These characteristics determine their suitability for various applications, composite manufacturing, and biodegradable plastics. The principal physical and mechanical properties of plant fibers include density, moisture absorption, tensile strength, Young's modulus, elongation at break, and thermal stability [19, 20]. Biofibers have been widely employed as reinforcements and fillers in composite materials [21]. They originate from biological sources and are

generally classified into non-woody (natural) fibers and woody fibers [22]. Natural fibers often demonstrate superior physical and mechanical performance compared with woody fibers due to their higher cellulose content, greater crystallinity, and lower density [21]. Consequently, their industrial relevance has continued to increase [23]. Ideal attributes of natural fibers include high specific strength and modulus, good processing flexibility, low weight, low cost, and excellent resistance to corrosion and fatigue [24].

There has been growing interest in developing bio-composites that incorporate thermoplastics as matrices reinforced with various fillers, such as fibers, nanoparticles, and additives. Thermoplastic matrices offer several advantages, including ease of processing, recyclability, and the capability to form complex geometries through manufacturing techniques such as injection molding, compression molding, and additive manufacturing. Bio-sourced composites provide enhanced mechanical properties, improved durability, and reduced environmental impact relative to conventional materials [25]. Bio-derived reinforcements are generally classified as fibrous or particulate, depending on their morphology and size. Fibrous reinforcements can be further divided into discontinuous reinforcements—comprising individual fibers or chopped bundles forming short fibers—and continuous reinforcements, which consist of long continuous fibers spun into yarns [26].

Plant fiber-reinforced composites (PFRCs) incorporate plant-based fibers, such as hemp, as reinforcements within a polymer matrix [27]. These materials offer advantageous physical properties, including sound absorption, thermal insulation, and electromagnetic wave attenuation, making them attractive alternatives to synthetic fiber composites [28]. Nevertheless, PFRCs exhibit sensitivity to moisture and temperature variations, which can affect their performance and long-term durability [29]. Despite these limitations, PFRCs have demonstrated high potential in a wide range of applications, with properties such as fire resistance, acoustic behavior, and vibration damping being extensively investigated [30]. These composites have been extensively characterized through rheological, optical, mechanical, and thermo-mechanical analyses to assess their overall performance [29]. PFRCs exhibit notable mechanical properties, together with distinctive chemical compositions and hierarchical structural arrangements [28]. Nevertheless, a major limitation of PFRCs is the strong variability in their physical and mechanical characteristics [31], combined with their pronounced sensitivity to moisture and their complex, often nonlinear, mechanical behavior. A key advantage of plant-based fibers over synthetic fibers lies in their low density. Most plant fibers are considerably lighter than common synthetic reinforcements such as glass fibers, with the exception of carbon fibers. For instance, hemp fibers have a density of approximately 1.4 g/cm³, compared with 2.5 g/cm³ for glass fibers [32], while carbon fibers typically range between 1.4 and 1.7 g/cm³. This inherent lightness significantly reduces the mass of final composite components—an important benefit for the automotive industry, where lighter vehicles improve fuel efficiency and reduce greenhouse gas emissions. Consequently, the use of plant fibers in automotive parts contributes directly to lower CO_2 emissions [33]. When plant fibers are combined with biodegradable matrices such as PLA, the resulting composites offer enhanced

biodegradability and recyclability compared with synthetic fiber composites, thereby reducing environmental impact at end of life [34]. Moreover, the production of plant fibers requires substantially less energy than that of synthetic fibers. Hemp and flax fibers require about 5 MJ/kg and 9.5 MJ/kg, respectively, whereas glass fiber production demands around 57.4 MJ/kg [34, 35]. In addition, plant fibers such as hemp and flax can be cultivated locally, supporting regional economic development and promoting sustainable agricultural practices [36]. From a mechanical standpoint, although the properties of plant-fiber composites vary across plant species and fiber grades, they generally remain inferior to those of synthetic fiber composites at equivalent reinforcement contents. Coroller [37] demonstrated that for injection-molded composites containing 30 wt.% short fibers, glass fibers provide significantly higher Young's modulus and tensile strength than plant fibers such as hemp, flax, bamboo, and sisal. This difference is further amplified by the optimized surface treatments applied to synthetic fibers, which enhance fiber–matrix adhesion and improve interfacial load transfer. AM, or 3D printing, is increasingly transforming the fabrication of thermoplastic composites, including those reinforced with plant fibers. This layer-by-layer process, driven by a digital model, offers unprecedented flexibility in design and customization. For plant-fiber-reinforced composites, AM involves extruding a thermoplastic filament loaded with natural fibers through a heated nozzle and depositing the material sequentially to form the final structure. This approach enables the creation of complex geometries with minimal material waste. However, to fully exploit the potential of these materials, challenges related to print resolution, fiber orientation control, and post-processing requirements must be addressed [38]. With the increasing demand for sustainable and high-performance materials, the integration of NFRPCs with AM technologies has attracted growing interest. This combination offers a promising route for producing lightweight, biodegradable, and customizable components, enabling the fabrication of complex geometries while maintaining environmentally responsible characteristics. Among AM techniques, FDM and extrusion-based 3D printing have become particularly relevant for processing NFRPCs, where natural fibers such as hemp are blended with thermoplastics like PLA to create filament or pellet-based feedstocks. However, 3D printing natural fiber composites presents several challenges. Mechanical performance can be compromised by defects such as residual stresses, uneven fiber distribution, and insufficient fiber-to-matrix bonding [39]. Additional factors include the choice of fiber type, volume fraction, and interfacial adhesion, all of which strongly influence composite properties [40]. As highlighted by Le Duigou [38], the moderate mechanical performance of printed parts is often linked to the low fiber aspect ratio required for extrusion through narrow nozzles, which limits effective load transfer and results in weaker composite structures. M. Milosevic et al. [41] demonstrated significant improvements in mechanical properties when 30 wt.% hemp or harakeke fibers were incorporated into polypropylene, reporting increases in tensile strength and Young's modulus of more than 50% and 143%, respectively. Similarly, B. Coppola et al. [42] observed that the incorporation of hemp powder into PLA reduced melt viscosity during compounding, influencing printability. Due to the short fiber lengths typically used in FDM, controlling fiber orientation remains critical for maintaining deposition quality. The microstructure and composition of plant fibers are also key determinants of

mechanical performance, with fiber surface properties strongly affecting interfacial adhesion and stress transfer. Poor fiber–matrix bonding in FDM-printed composites frequently leads to extrusion-related defects such as porosity, which in turn reduce stiffness and strength. Chemical surface treatments, including alkali, acetic anhydride, maleic anhydride, and silane treatments, have been shown to enhance interfacial adhesion. Sawpan et al. [43] reported increased interfacial shear strength for most treated PLA/hemp systems—up to 11.4 MPa for alkali-treated fibers—and even higher values in UPE/hemp composites, reaching 20.3 MPa for fibers treated with combined Na-OH and silane. Defect minimization is therefore essential, as defects such as porosity and delamination substantially degrade mechanical properties. Strategies to reduce porosity include vacuum drying of fibers, strict control of printing humidity and temperature, and the use of plasticizers such as PEG, although PEG contents above 10 wt.% can reduce tensile strength [44–46]. Fiber content also plays a critical role: Sawpan et al. [47] found that increasing hemp fiber content from 0 to 30 wt.% in PLA composites enhanced tensile strength and Young's modulus, and substantially increased flexural modulus. Impact strength improved up to 20 wt.% but deteriorated at higher contents due to increased porosity and reduced interfacial bonding [48]. Fiber loadings above 20 wt.% may also cause excessive melt viscosity, resulting in non-uniform extrusion and poor interlayer adhesion [49]. Fiber aspect ratio further influences reinforcement efficiency. Low aspect ratios limit load transfer and may cause debonding rather than effective stress transmission [38], whereas higher aspect ratios enhance mechanical performance [50]. However, aspect ratio selection is constrained by nozzle diameter, as long fibers can cause clogging and dispersion issues. Moisture management is another critical factor. Plant fibers and some bio-based polymers such as PLA are moisture-sensitive, which can lead to printing defects and material degradation. As reported for flax fibers [51], moisture uptake weakens the fiber–matrix interface and compromises composite quality. Kariz et al. showed that increasing moisture content (33–87%) reduced the stiffness of wood/PLA composites. Moisture present during processing may vaporize, generating porosity and adhesion problems [52], altering crystallinity [53], and creating internal stresses that cause warping [38]. During service, moisture sensitivity can impair dimensional stability and damage the fiber–matrix interface [54, 55]. Therefore, rigorous drying and conditioning prior to processing are essential [56, 57]. Finally, local pre-deposition heating has been shown to enhance interlayer adhesion in FDM-printed PLA. Yu et al. [58] demonstrated that such auxiliary heating improved tensile strength from 38.4 MPa to 63.6 MPa and reduced mechanical anisotropy from 0.51 to 0.22, reflecting a substantial improvement in structural integrity.

PLA is recognized as an environmentally friendly material due to its versatility, as it can be recycled, incinerated, composted, or safely landfilled. Its production also requires 25–55% less energy than conventional polymers, reinforcing its sustainability [59]. Natural fibers such as flax, hemp, jute, kenaf, and ramie are commonly used in AM filaments [60, 61, 62]. When combined with PLA, these fibers create fully renewable filaments, enhancing the environmental performance of additive manufacturing.

Chemically treated fibers further improve functional properties, supporting sustainable material development in both academia and industry.

Life Cycle Assessment (LCA) is a standard method for evaluating the environmental impacts of products or processes [63, 64]. Cradle-to-grave LCA examines the full life cycle, while gate-to-gate or gate-to-grave focus on production-to-use or production-to-disposal impacts. The methodology involves four steps: goal and scope definition, inventory analysis, impact assessment, and result interpretation [64]. Specialized software, with comprehensive material and process databases, is often used to streamline calculations.

Hemp-based filaments have lower environmental impacts than synthetic alternatives, particularly for Cumulative Energy Demand, Global Warming Potential, and Abiotic Depletion Potential, making them a sustainable alternative to glass fiber-reinforced polymers [60, 65]. Comparative LCAs using tools like Umberto NXT and SimaPro, along with databases such as ecoinvent and methods like ReCiPe, CML, or IMPACT 2002+, show that raw material extraction dominates PLA's environmental footprint, notably in freshwater ecotoxicity and water depletion [60, 66, 67].

The present study investigates the thermo-rheological and mechanical behavior of PLA-based biocomposites. The compositional and chemical structure of the PLA/Hemp/PEG system was characterized using Fourier-transform infrared spectroscopy (FTIR). Subsequently, the 3D printing process was optimized through a design of experiments approach, producing sets of printed plates to evaluate the influence of nozzle temperature, printing speed, and layer thickness on surface quality and porosity. Mechanical characterization of the printed parts was performed via tensile testing to assess the mechanical performance of PLA/Hemp/PEG. Finally, an LCA was conducted to evaluate the environmental impact of the biocomposites, considering six levels of component-specific analysis.

2. Materials and methods

This section focuses on descriptions of the materials used in 3D printing and the various characterization methods.

2.1. Materials

2.1.1. Properties of PLA

PLA (PLI 005) is a specialized PLA pellet grade designed for a variety of thermoplastic manufacturing processes. It is provided by Natureplast (Mondeville, France), a company specializing in bioplastics. PLA exists in several isomeric forms, mainly PLLA (poly-L-lactic acid) and PDLA (poly-D-lactic acid). PLA PLI 005 is primarily made of PLLA, which has a semicrystalline structure that offers the mechanical strength and stability required for injection molding and blow molding applications. Table 1 summarizes the properties of PLA PLI 005.

Table 1: properties and characteristics of PLA PLI 005

Property	Value
Bio-based content	100 %
Density	1.25 g/cm^3
MFI	25- 35 g/10 min
Melting temperature (T_m)	169 – 179 °C
Tensile modulus	3500 MPa
Elongation at break	4 %

2.1.2. Properties of the PLA/Hemp/PEG composites

Hemp fibers are natural materials obtained from the Cannabis sativa plant. They are long, strong, and durable, with fiber bundles ranging from a few centimeters up to several tens of centimeters. Hemp fibers are valued for their tensile strength, light weight, and environmentally friendly cultivation, which typically requires minimal or no pesticides.

The PLA/Hemp composite retained in this work was provided by Automotive Performance Materials (Dijon, France). It is produced on an industrial line designed for large-scale manufacturing of composite pellets, featuring a twin-screw extruder with multiple dosing units and a granulator to ensure uniform quality. This facility delivers ready-to-use blends for automotive applications, using regionally sourced agricultural fibers. The matrix material is PLA, reinforced with 20 wt% short hemp fibers.

The PLA–Hemp pellets initially supplied by APM contained 30 wt% hemp without additives, which led to poor extrudability and unstable flow during printing. In order to obtain a formulation suitable for P-MEX, the fibre content was reduced to 20 wt% and several additives were screened (different PEG

molecular weights and stearic acid) to facilitate mixing extrusion and printing processes. Internally, PEG content was varied from 0 to 10 wt% in 2.5 wt% increments, but rheological shear curves largely overlapped, indicating only limited additional benefit beyond 5 wt% in terms of viscosity reduction and flow behavior. This is consistent with literature showing that PEG improves PLA processability but that higher PEG contents can detrimentally affect mechanical performance and morphology by excessive plasticization or phase separation. A PEG content of 5 wt% was therefore selected as a compromise: sufficient to ease extrusion and printing of the 20 wt% hemp composite, while limiting the risk of degradation of mechanical properties. On this basis, the objective of the present work was to optimize processing parameters for this reference formulation, rather than to perform a full optimization of PEG content.

Polyethylene Glycols (PEG) from Merck KGaA (Allemagne) is chosen as plasticizer for composite formulations. PEG 1500 improves process ability and flexibility with its moderate molecular weight. This material ensures uniform dispersion and facilitate the extrusion and molding process, optimizing mechanical properties. The properties of PEG are shown in Table 2.

The binder was formulated using 75 wt% PLA PLI 5 and 20 wt% Hemp and 5 wt% additive.

Table 2: PEG description and properties

Additive	Density (g/cm^3)	Tm (°C)
PEG 1500	1.2	43 - 49

2.2. Methods

2.2.1. Rheological behavior of PLA/Hemp/PEG biocomposites

A comprehensive series of rheological tests was conducted to fit the experimental data to the Carreau-Yasuda model. The shear viscosity of molten PLA/Hemp (above its melting temperature) was measured using a rotational cone-and-plate rheometer over both low and high shear rates, within a temperature range of 190 - 210 °C. For PLA/Hemp/PEG, measurements were performed at shear rates from 1 to 500 s^{-1} to evaluate the effect of shear rate on viscosity. Each test was repeated three times to ensure reproducibility.

Rheological characterization was carried out with a Thermo Fisher Scientific HAAKE MARS III rotational rheometer (Thermo Fisher Scientific, Illkirch-Graffenstaden, France) in oscillatory dynamic (frequency sweep) mode, using a cone-and-plate setup with a 2° angle. The biocomposite sample was placed between a stationary disk and a coaxial cone of equal radius. The cone was rotated around the shared axis at a controlled angular velocity, while the sample on the lower disk was gradually positioned to the required gap. All tests were replicated three times to guarantee consistent and reproducible results. The rheological model involved in the Carreau-Yasuda law is represented by Eq. (1):

$$\eta = \eta_\infty + (\eta_0 - \eta_\infty)\left(1 + \left(\lambda\dot{\bar{\gamma}}\right)^a\right)^{\frac{n-1}{a}} \quad (1)$$

where $\eta_0$is the zero-shear rate viscosity, λ is the characteristic Newtonian-to-pseudoplastic transition time of the polymer, the parameter a reflects the transition curvature between the Newtonian plateau and the decreasing asymptote of the power law, n is the pseudo-plasticity index and $\dot{\bar{\gamma}}$ is the generalized shear rate.

2.2.2. Manufacturing processes

In this study, the COGIT printer was employed to print structures in PLA/Hemp/PEG, Figure 1. The COGIT 3D printer (COGIT Composites, France) is a high-precision additive manufacturing system capable of producing complex geometries directly from digital designs. It offers excellent reproducibility and supports a variety of materials for both prototyping and functional uses. With its integrated hardware and software optimizations, the printer ensures accurate layer deposition, structural consistency, and reliable operation, making it a versatile tool for research, engineering, and experimental applications in additive manufacturing.

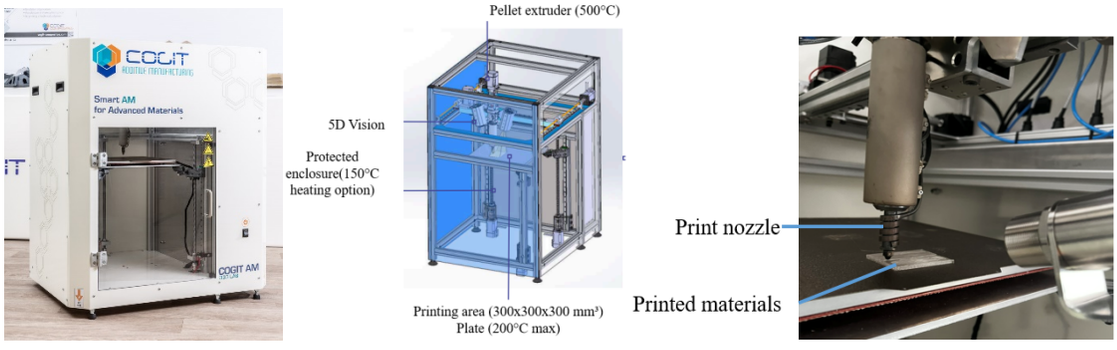

Figure 1: COGIT AM's 3D printer.

The technical and thermal properties of the equipment used are detailed in Table 3.

Tableau 3: Technical Specifications of the 3D Printer.

Parameters	**Fused Granular Fabrication**
Material packaging	Granules or Filaments
Print volume	300 x 300 x 300 mm³
Maximum extrusion temperature	500 °C
Maximum temperature of the plate	200 °C
Maximum number of extruders	1
Maximum print speed	100 mm/s
Movement accuracy	X, Y : 10 µm / Z : 2µm
Layer thickness	Mini 100 µm
Nozzle size	From 0.4 to 1.2 mm
Dimensions (L x W x H)	800 x 700 x 1050 mm³

2.2.3. Printing optimization methodology

To optimize 3D printing parameters involving three factors, each at three levels, the L9 Taguchi orthogonal array is used. This array offers an efficient and balanced approach to evaluate the effects of each factor individually and in combination with others. Orthogonal experiments are a structured experimental design widely used in engineering, statistics, and manufacturing. Their main purpose is to identify which factors most significantly influence a specific response. This is achieved by systematically varying the factors in a controlled manner to maintain orthogonality while reducing the total number of experiments. Each factor is tested at the same number of levels, and the initial optimization focuses on minimizing the adverse effects of porosity.

The porosity (Pc) of the sample, which indicates the percentage of voids or pores within the material, is calculated using the Eq. (2). To accurately assess the properties of the 3D-printed sample, the procedure begins by measuring its actual weight using a precise analytical scale, which provides the printed weight, denoted as P_{wt}:

$$P_c(\%) = \left(1 - \frac{P_{wt}}{T_{wt}}\right) \times 100 \quad (2)$$

The theoretical weight (T_{wt}) of the sample is then calculated using the formula $T_{wt} = V \times \rho$. This theoretical weight represents the weight the sample would have if it were free of any internal voids or pores.

2.2.4. Rheology coupled to fast-scan FTIR spectroscopy

FTIR combined with rheology enables real-time monitoring of the kinetic evolution of reactive systems. Integrating both techniques in a single instrument allows the rheological behavior to be directly correlated with molecular-scale structural changes, particularly the vibrations of functional groups in chemical bonds. The FTIR spectrometer operates at high acquisition speeds, capturing the onset of reactions simultaneously with rheological measurements. This setup, known as RHEONAUT, combines a Thermo Scientific Haake MARS III rheometer (Thermo Fisher Scientific, Illkirch-Graffenstaden, France) with a 20 mm parallel-plate geometry featuring a transparent window, and a Nicolet IS10 FTIR spectrophotometer equipped with a specialized acquisition system. Mid-infrared spectra (400–4000 cm^{-1}) were recorded at a resolution of 4 cm^{-1}, with each spectrum representing 32 scans. The module uses a single-reflection diamond ATR (attenuated total reflection) optical unit with an integrated electrical heater, enabling studies of molten polymers up to 400 °C. Infrared radiation passes through the crystal to the sample interface, where it is partially absorbed and reflected, then redirected to the detector using mirrors and lenses for precise measurement.

2.2.5. Mechanical characterization

Tensile testing was carried out at room temperature using an MTS Criterion Model 45 universal testing machine (MTS Systems Corporation, Créteil, France) fitted with a 5 kN load cell and contact extensometers. A constant crosshead speed of 2 mm/min was applied. The specimens, designed

according to ISO 527-4 type 1B geometry (Figure 2), were laser-cut from printed parallelepiped samples to ensure high dimensional precision and smooth surfaces suitable for transverse extensometer measurements. The mean values of Young's modulus, tensile strength, and fracture strain were obtained in accordance with the ISO 527 standard, with Young's modulus evaluated over a strain interval ranging from 0.05 % to 0.25 % (Figure 3).

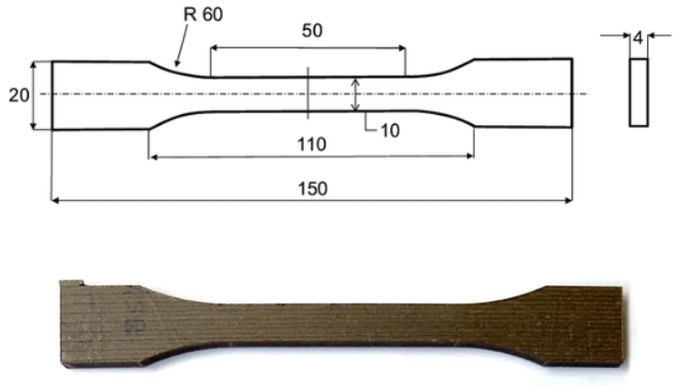

Figure 2: ISO 527-4 type 1B sample dimensions

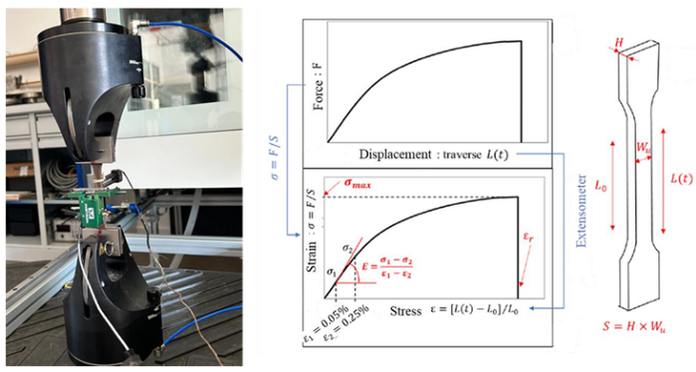

Figure 3: MTS machine testing and tensile methodology

2.2.6. Life cycle assessment of PLA/Hemp/PEG

LCA is a systematic method used to evaluate the environmental impacts of a product, process, or service throughout its entire life cycle. It considers all stages, from raw material extraction to production, use, and end-of-life. LCA helps identify opportunities to reduce environmental impacts and support sustainable decision-making.

The system boundaries take the creadle-to-gate with the production of PLA, Hemp fiber and composite. The Hemp fiber is modeled as flax fiber with the same production efficiency. The French mix is used to produce the hemp fiber and the composite. The LCA is carried out with the use of OpenLCA software 2.3.1 and Ecoivent v3.5 and the environmental impacts are calculated with EF 3.0.

3. Results and discussions

3.1. Rheology and identification

The measures of shear viscosity as a function of the shear rate and temperature are displayed in Figure 4. The curves clearly exhibit a thermo-dependent pseudoplastic behavior since viscosity decreases as a function of temperature and shear rate.

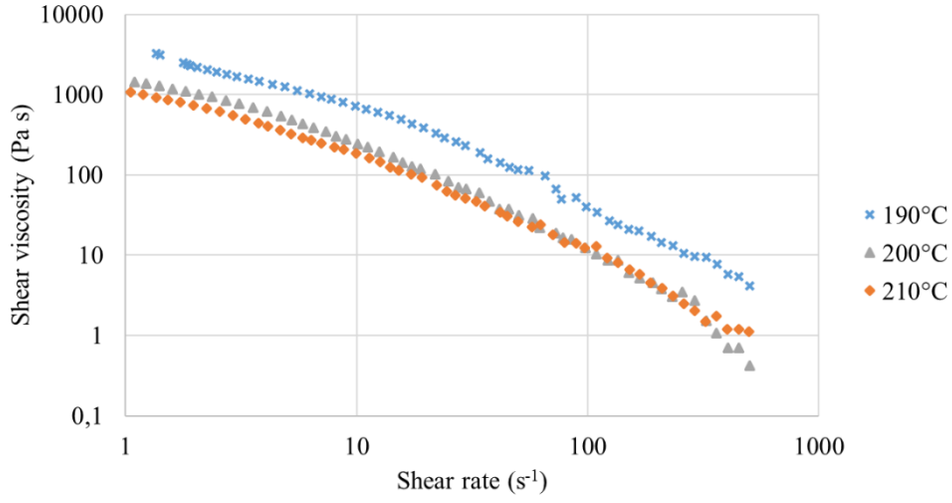

Figure 4: Experimental shear viscosity of PLA/Hemp/PEG versus shear rate and temperature.

The values of the identified parameters were obtained by the least square method with the MATLAB software using the experimental data and are summarized in Table 4:

The value n < 1 confirms the pseudoplastic behavior of the PLA/Hemp composite. $\eta\infty$ was set null at high shear rate according to the observed vanishing viscosity. As temperature increases, $\eta 0$ and λ decrease, while n and a slightly increase, according to usual time temperature correspondence between the interaction time and temperature involving a time scaling and temperature scaling equivalence in shear viscosity, relaxation time, and conservation modulus curves.

Table 4: Carreau-Yasuda model parameters identified for PLA/Hemp/PEG composites.

T **(°C)**	η_0 **(Pa s)**	η_∞	λ **(s)**	***n***	***a***
190	3000	0	0.25	0.35	2
200	1500	0	0.125	0.45	2.2
210	900	0	0.06	0.50	2.5

3.2. Optimization of printing process

Producing dense parts from different formulations requires thorough optimization of printing parameters. Key factors affecting print quality include nozzle and bed temperature, nozzle diameter, and printing speed. Nozzle temperature primarily influences the material's viscosity, while printing speed controls the extrusion flow rate. Among these, nozzle temperature, layer height, and printing speed are critical, whereas other parameters have a smaller impact and can be fixed. Optimization of these

parameters was conducted under the specific test conditions listed in Table 5, focusing on maximizing part density and ensuring geometric accuracy.

Table 5: Printing parameters for optimization of PLA/Hemp formulations

Levels	Nozzle Temperature (°C)	Layer Thickness (mm)	Printing Speed (mm/s)
1	190	0.3	30
2	200	0.4	40
3	210	0.5	50

The effects of three factors were explored at 3 levels each mainly, the printing temperature, the layer height and the printing speed, Figure 5. The infill is held at 100 % and the nozzle diameter selected is 1 mm with a bed temperature at 50 °C.

The L9 Taguchi design clearly identifies main effects: fiber content (dominant, 7 - 13 % porosity rise at 20 wt% due to fiber-induced voids); nozzle temperature (decrease in porosity due to better adhesion and stabilization close to 200 °C); layer height (positive correlation, thicker layers increase voids); printing speed (minor effect 30 - 50 mm/s). These align with literature on FDM porosity drivers.

Optimal settings (200 °C, intermediate layer height, 35 mm/s, 20 wt% fiber) minimize porosity by balancing melt flow for interlayer diffusion without fibre degradation. As a conclusion, L9 orthogonal arrays prioritize main effects over interactions, which are confounded and difficult to resolve reliably.

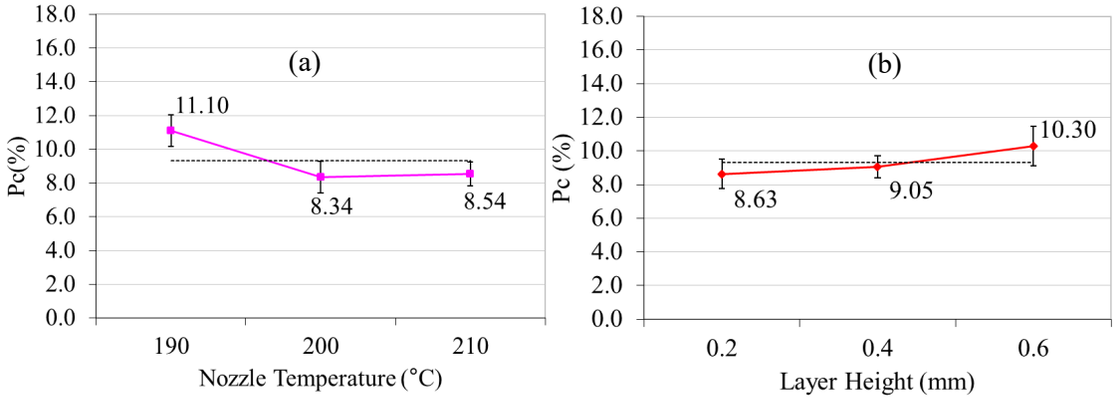

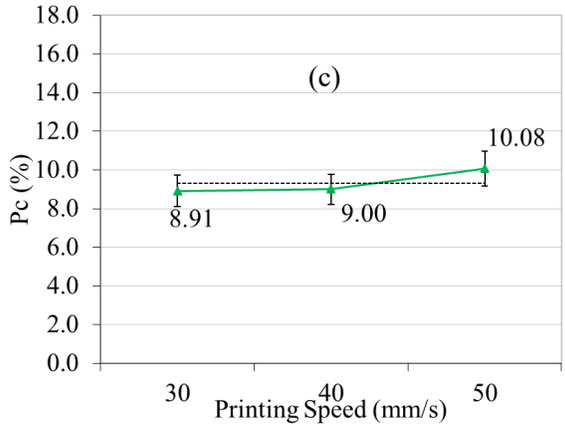

Figure 5: Effects of factors from DOE (Taguchi method) a) printing temperature, b) layer height and c) printing velocity.

Figure 5 (a) shows the influence of nozzle temperature on porosity. When the temperature is increased from 190 °C to 200 °C, porosity decreases from 11.10% to 8.34 %. Increasing the temperature further to 210 °C results in a slight rise in porosity to 8.54 %. The small difference between 200 °C and 210 °C indicates that the effect of nozzle temperature on porosity reduction may plateau or slightly reverse at higher temperatures. This behavior could be due to minor variations in thermal control during printing, causing small fluctuations in porosity. Overall, the most significant decrease in porosity occurs between 190 °C and 200 °C, highlighting this range as critical for improving layer consolidation.

Figure 5 (b) illustrates the relationship between layer height and porosity. Porosity increases from 8.63% to 10.30 % as the layer height is raised from 0.2 mm to 0.6 mm. This suggests that thicker layers may lead to higher porosity, potentially due to less accurate layer deposition and weaker interlayer bonding. While the error bars show some overlap, indicating measurement variability, the overall trend of increasing porosity with greater layer height remains consistent and should be considered when optimizing printing parameters.

Figure 5 (c) illustrates the effect of printing speed on porosity. Porosity remains approximately 9 % at speeds of 30 mm/s and 40 mm/s, with a slight increase to 10 % at 50 mm/s. This suggests that, within the tested range of 30 - 50 mm/s, printing speed has a relatively minor influence on porosity compared with factors such as fiber content or nozzle temperature. However, as the data are limited to three points and the variations are small, this trend should be interpreted cautiously. Overall, the impact of printing speed on porosity appears to be limited within this range.

The print settings employed in this study are shown in Table 6.

Table 6: Print parameters for PLA/Hemp/PEG

Layer height	0.5 mm
Fill rate	100 %
Fill pattern	Rectilinear
Upper heating zone temperature	190 °C
Middle heating zone temperature	195 °C
Nozzle temperature	200 °C
Bed temperature	50 °C
Print speed	35 mm/s

The influence of temperature on print quality is shown in Figure 6. With the same print speed and layer thickness, the sample printed at 200 °C has a higher surface quality than those printed at 190 °C and 210 °C. The raster angles of ± 45° were initially selected because they are widely used in literature as a reference orientation for evaluating the mechanical and process behavior of 3D-printed composites and polymers. This bidirectional pattern provides a balanced in-plane stress distribution and allows assessment of the material's performance under multi-directional loading. Using ± 45° orientations during the parameter optimization phase ensured that the process settings (layer height, flow rate, temperature, etc.) were not biased toward a single fiber or filament direction. Once the optimal parameters were identified, additional samples printed at 0° and 90° were tested to analyze the influence of orientation, with the 0° configuration showing superior properties.

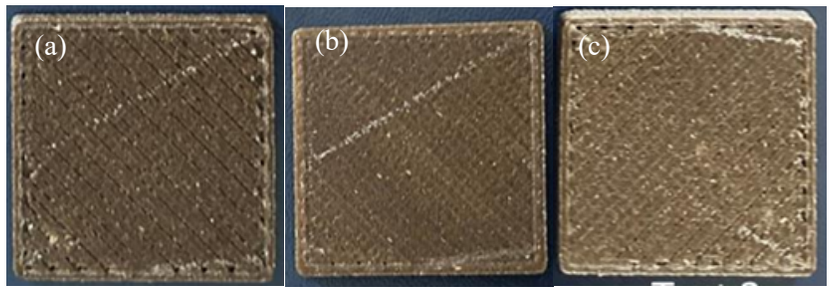

Figure 6: Printed samples in the extrusion temperature range of (a) 190 °C, (b) 200 °C and (c) 210 °C.

3.3. FTIR spectroscopy

The 3D printed PLA/Hemp/PEG biocomposites were subjected FTIR analysis to evaluate the chemical constituents at different temperatures (190 °C, 200 °C and 210 °C), Figure 7. Analysis of the results shows the presence of O-H bonds, it confirms the presence of the cellulose and hemicellulose which belongs to the hemp fibers.

C=O indicates the bonding between the PLA and hemp hydroxyl group depicting better interfacial compatibility between the constituents.

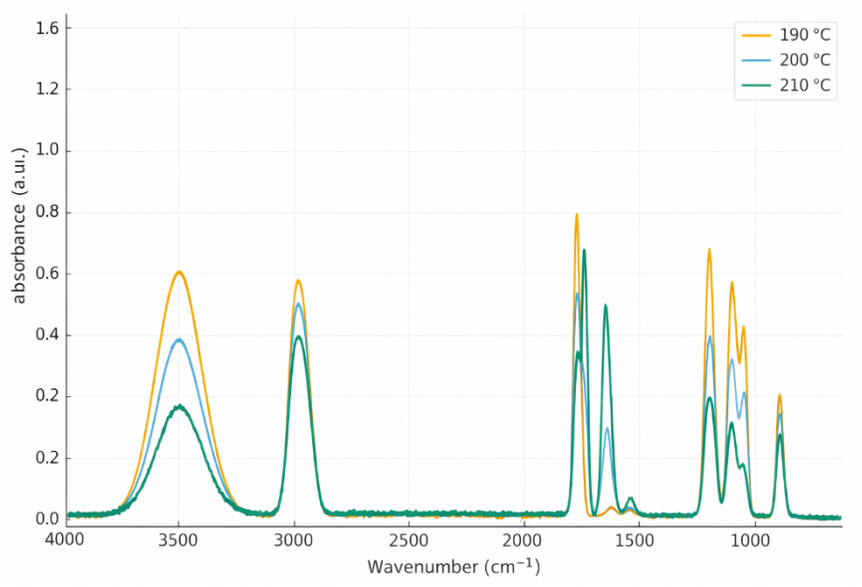

Figure 7: FTIR spectra of PLA/Hemp biocomposites at 190°C, 200°C and 210°C.

The FTIR spectra recorded at 190 °C, 200 °C, and 210 °C reveal progressive chemical modifications within the PLA/hemp biocomposite as temperature increases. A pronounced decrease of the broad O–H stretching band around 3500 cm^{-1} is observed, reflecting dehydration and the gradual degradation of hydroxyl-rich cellulose and hemicellulose in the hemp fibers. The aliphatic C–H stretching region between 3000–2850 cm^{-1} also diminishes steadily with temperature, indicating increasing scission of PLA chains, particularly those involving methyl substituents. The characteristic PLA ester carbonyl peak at ~1750 cm^{-1} shows a strong decline from 190 °C to 210 °C, confirming extensive chain cleavage, while a new peak around 1715 cm^{-1} grows in intensity, consistent with the formation of oxidized carbonyl species such as ketones, carboxylic acids, and terminal degradation products. Simultaneously, the absorption band near 1620 cm^{-1} becomes more pronounced at higher temperatures, likely arising from conjugated C=C structures formed during hemicellulose pyrolysis and partial transformation of lignin, as well as unsaturated degradation fragments. Additional temperature-dependent reductions in the C–O–C and C–O stretching bands in the 1180–1080 cm^{-1} and ~1030 cm^{-1} regions reflect depolymerization of PLA and cleavage of polysaccharide glycosidic linkages. Finally, a noticeable elevation of the baseline at 210 °C—particularly in the lower wavenumber region—suggests the formation of char, thermally induced aromatic conjugation, and oxidation byproducts, collectively confirming advanced thermal degradation of both the polymer matrix and the natural fibers.

Table 7 shows the prominent spectral peaks, their chemical structure in the form of a functional group for PLA/Hemp biocomposites.

Table 7: Summary of FTIR Spectra for PLA/Hemp/PEG biocomposites (190 → 210 °C)

Wavenumber Region	Functional Group	Trend (190→210 °C)	Interpretation

~3500 cm^{-1}	OH	↓ strong decrease	dehydration + cellulose degradation
3000–2850 cm^{-1}	C–H	↓ slight/moderate	PLA chain scission
1750 cm^{-1}	C=O (PLA ester)	↓ significant	PLA depolymerization
1715 cm^{-1}	C=O (degradation)	↑	oxidized carbonyls (acids/ketones)
~1620 cm^{-1}	C=C	↑	conjugated and lignin-derived structures
1180–1080 / 1030	C–O–C / C–O	↓	degradation of PLA & polysaccharides
—	Baseline	↑	carbonaceous residue (char) formation

3.4. Mechanical behavior

The mechanical behavior of the PLA/Hemp composites under tensile loading is summarized in Figure 8. The strain stress curves corresponding to three repetitive tests for two materials (PLA-20H and and PLA-20H-PEG). This behavior is typical of natural-fiber-reinforced polymers with quasi-brittle progressive tensile failure. The mechanism is dominated by matrix cracking, interfacial debonding, and fiber pull-out. The tensile test results indicate that the addition of hemp (PLA-20H) and the combined incorporation of hemp with PEG (PLA-20H-PEG) slightly influence the mechanical properties of PLA. The tensile strength remains relatively constant across all samples, with PLA, PLA-20H, and PLA-20H-PEG exhibiting values around 40 MPa, suggesting that the fillers do not significantly compromise the strength of the matrix.

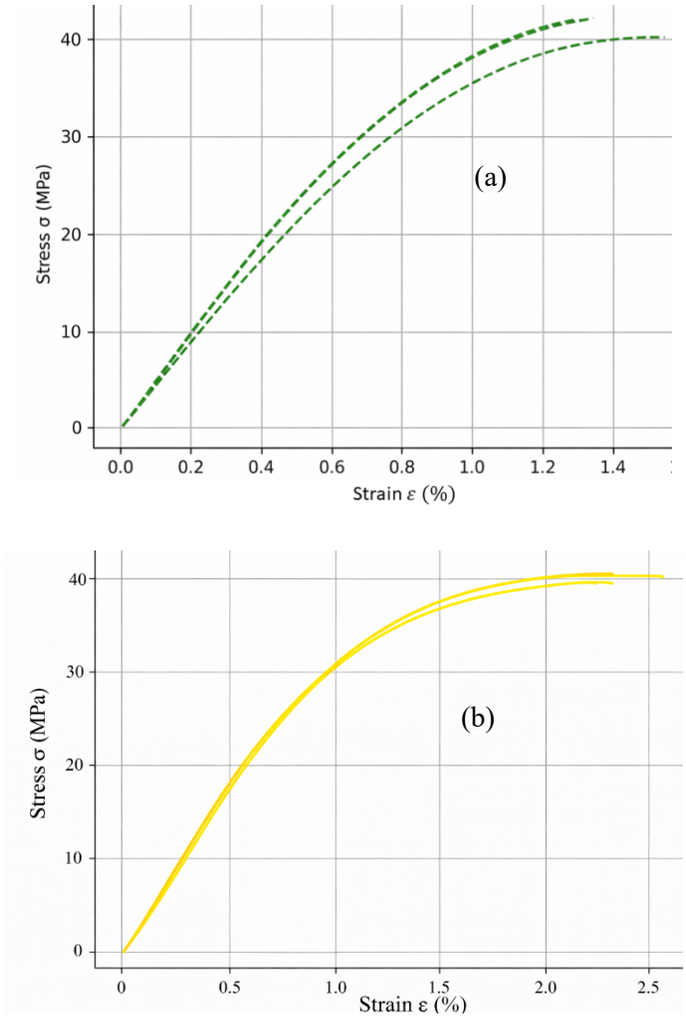

Figure 8: Influence of additives on the tensile properties of the pellet-based material extrusion of the formulations (a) PLA-20H and (b) PLA-20H-PEG.

In terms of stiffness, measured by Young's modulus, both PLA-20H and PLA-20H-PEG show a noticeable increase compared to neat PLA, indicating that the incorporation of hemp fibers enhances the rigidity of the composite. Specifically, Young's modulus increases from approximately 3.5 GPa for PLA to about 5 GPa for the modified composites, Figure 9.

Elongation at break demonstrates the most pronounced effect of PEG addition. While PLA and PLA-20H display similar ductility (~1.35%), the PLA-20H-PEG composite exhibits a higher elongation at break (~2.5%), indicating that PEG acts as a plasticizer, improving the flexibility of the material without compromising tensile strength.

As a conclusion, the results suggest that the PLA-20H-PEG composite achieves a balanced combination of strength, stiffness, and ductility, making it a promising material for applications requiring both mechanical performance and enhanced flexibility. The PLA–hemp composite exhibits a nonlinear tensile response with progressive damage characterized by matrix cracking, fiber–matrix debonding, and fiber pull-out, leading to quasi-brittle failure.

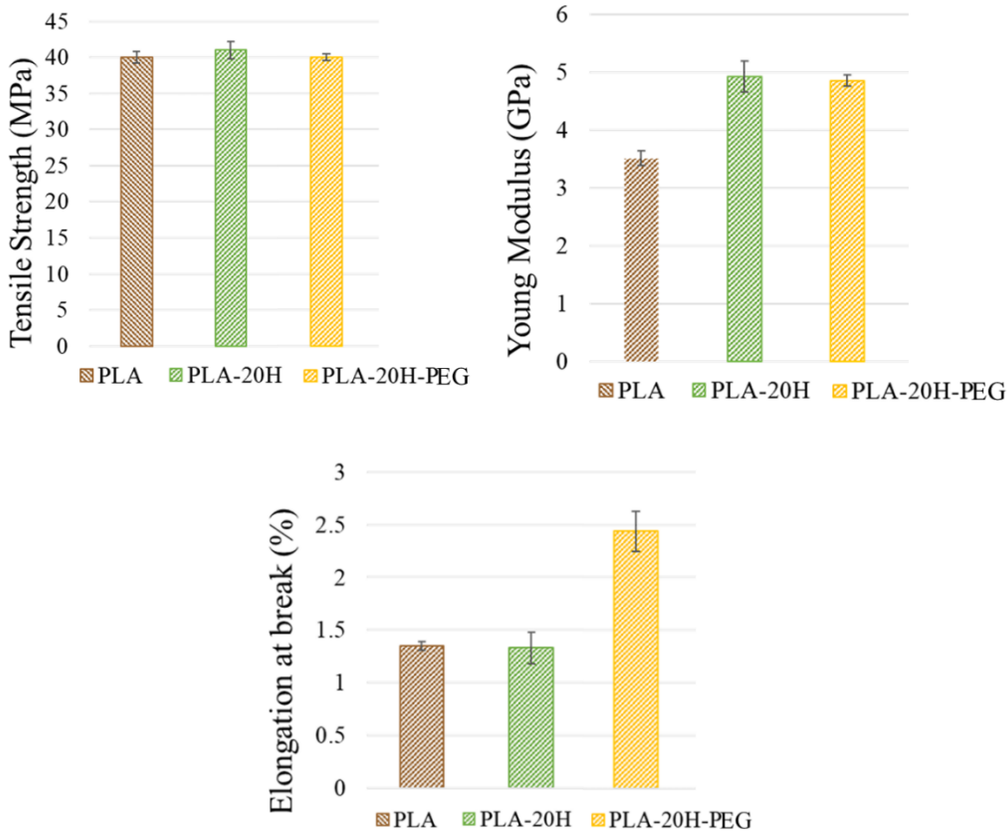

Figure 9: Tensile strength and Young's modulus values and Elongation at break of PLA, PLA-20H and PLA-20H-PEG.

The different mechanical properties of composites are presented in Table 8.

Table 8: Tensile properties of PLA, PLA-20H and PLA-20H-PEG

	PLA	PLA-20H	PLA-20H-PEG
E (GPa)	3.5 ± 0.50	4.9 ± 0.27	4.85 ± 0.10
σ (MPa)	40 ± 1	41 ± 1.17	40 ± 0.48
ε (%)	1.35 ± 0.15	1.3 ± 0.15	2.4 ± 0.19
ν	0.35 ± 0.02	0.38 ± 0.02	0.36 ± 0.02

3.5. LCA of PLA/Hemp: Contribution analysis by process/component (per kg)

The functional unit (FU) chosen for the LCA study is mass (kg). For one FU of material, the composition consists of 0.75 kg of PLA, 0.20 kg of hemp fiber, and 0.05 kg of plasticizer. In addition to the material inputs, the process requires an energy consumption of 99.900 kJ per FU.

Table 9 summarizes the environmental impacts of the composite material assessed using the EF 3.0 method and normalized per functional unit of composite mass. The climate change impact, expressed as

GWP100, is 5.18 kg CO_2 equivalent. The depletion of energy resources (ADP) amounts to 364.07 MJ. Acidification potential is estimated at 0.034 mol H^+ equivalent, while photochemical oxidation reaches 0.020 kg NMVOC equivalent. Water use associated with the functional unit is 11.22 m^3, and land use, expressed by the Soil Quality Index (SQI), is 92.40.

Table 9: The environmental impacts with EF 3.0 method

	FU per composite mass (kg)
Climate change GWP100 (kg CO2eq)	5.18
Energy resources ADP (MJ)	364.07
Acidification AE (mol H+ eq)	0.034
Photochemical oxidation (kg NMVOC eq)	0.020
Water use (m^3)	11.22
Land use SQI (-)	92.40

Table 10 summarizes the percentage contribution of four system elements—PLA/Hemp/PEG composites, PLA (polymer matrix), hemp fiber, and PEG (additive)—to six environmental impact categories on a per-kilogram basis. Figures 9–14 show the component contributions for each impact category, and Figure 15 presents a stacked comparison across all categories.

Table 10: The contribution processes in the environmental impacts (%): per kg

	PLA/Hemp/PEG composites	PLA	Hemp fiber	PEG
Climate change GWP100 (kg CO_2-eq)	48.29	46.47	3.21	2.04
Energy resources -ADP (MJ)	91.13	7.8	0.37	0.7
Acidification AE (mol H+ eq)	49.69	44.04	4.94	1.32
Photochemical oxidation (kg NMVOC eq)	45.70	47.76	4.91	1.73
Water use (m^3)	35.94	40.57	23.13	0.36
Land use SQI (-)	17.92	28.01	53.86	0.21

The contributions to global warming potential (GWP100), Figure 10, are dominated by printing PLA/Hemp/PEG composites (48.29 %) and PLA production (46.47 %), with hemp fiber and PEG together contributing only ~5.3 %. This indicates that emissions related to electricity or thermal energy use during printing and the cradle-to-gate emissions of PLA (feedstock cultivation, fermentation, and polymerization) are the principal drivers of the carbon footprint for the studied composite. Any mitigation strategy aiming at GWP reduction should therefore first target machine energy consumption

(e.g., energy-efficient printing, process optimization, or low-carbon electricity) and secondarily raw material selection or low-GWP PLA supply chains.

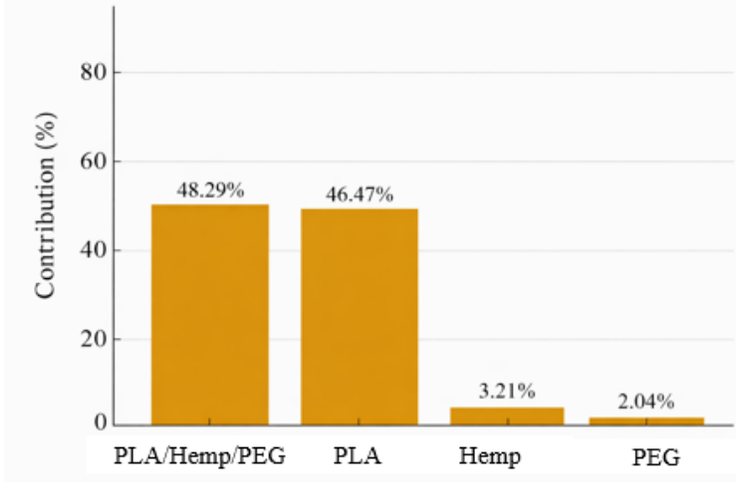

Figure 10: Contribution to climate change GWP100 (Kg CO_2eq)

Energy-resource depletion is overwhelmingly attributed to printing PLA/Hemp/PEG composites (91.13 %), while PLA accounts for only 7.8 % and the other components are negligible, Figure 11. This shows that the operation-phase (electricity, heating) of the printer is by far the most energy-intensive stage for a kilogram of printed composite. Reducing printing energy per mass (e.g., higher deposition rates, batch printing, and optimized process parameters) or switching to renewable electricity would substantially lower the ADP indicator.

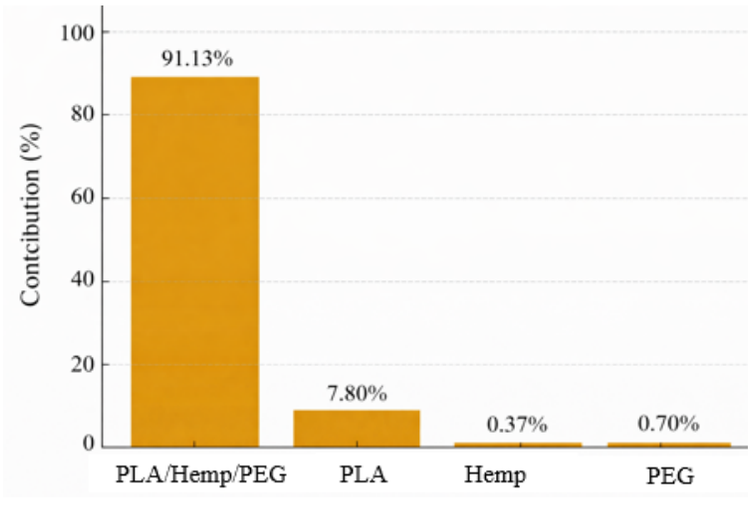

Figure 11: Contribution to energy resources - ADP (MJ)

Acidification potential is split primarily between printing PLA/Hemp/PEG composites (49.69 %) and PLA (44.04 %), mirroring the pattern observed for climate change. These contributions likely stem from fossil-fuel combustion and industrial emissions in both energy supply and PLA production pathways (e.g., fertilizer use or combustion emissions during feedstock processing). Targeted emission controls in feedstock cultivation and energy production could therefore reduce acidifying emissions.

Photochemical oxidation (precursor emissions for tropospheric ozone) is almost evenly split between PLA (47.76 %) and 3D printing (45.70 %), with hemp fiber and ethylene glycol minor. The significant role of PLA suggests that volatile organic compound emissions during feedstock processing or polymer manufacturing contribute meaningfully to smog formation potential.

Water consumption differs from the previously discussed categories: PLA (40.57 %) and printing PLA/Hemp/PEG composites (35.94 %) are both significant, but hemp fiber accounts for a notable 23.13 %, Figure 12. This reflects agricultural water needs in hemp cultivation as well as water used in PLA feedstock (e.g., irrigation in biomass production). For water-limited regions, material sourcing (choice of feedstock, irrigation practices) and process water management are crucial.

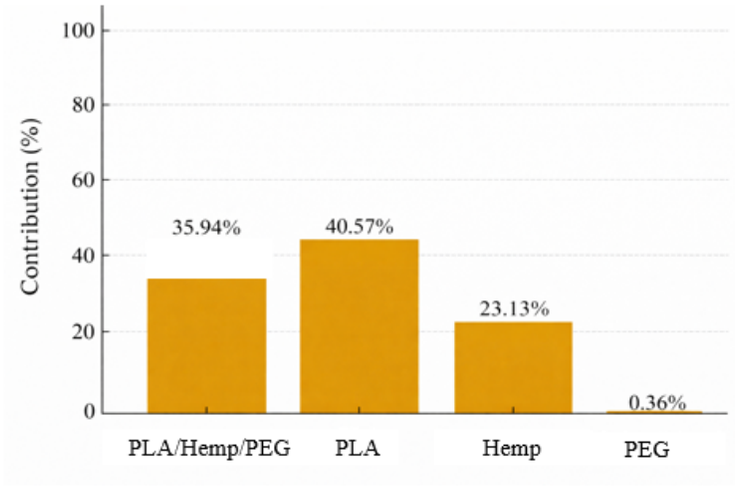

Figure 12: Contribution to water use (m^3)

The hemp fiber dominates land use (53.86 %), followed by PLA (28.01 %) and printing PLA/Hemp/PEG composites (17.92 %). This strong dominance of hemp in land occupation arises from the agricultural land required for fiber production. If land-use minimization is a priority (biodiversity or food-land competition concerns), strategies may include using agricultural residues, higher-yield fiber crops, or sourcing hemp from low-impact land types.

Printing PLA/Hemp/PEG composites is the single largest contributor to energy-related impacts and is a major contributor for climate, acidification, and photochemical oxidation. PLA is consistently a major contributor across most impact categories, particularly climate, photochemical oxidation, water use, and land use. Hemp fiber contributes disproportionately to land use and significantly to water use, but negligibly to energy and climate categories. PEG has only minor contributions across all categories for this system.

If the objective is to lower GWP and ADP simultaneously, prioritize interventions on the printing of PLA/Hemp/PEG composites (energy use reduction, machine efficiency, renewable electricity). If the objective targets land and water footprint, focus on fiber sourcing (agricultural practice improvements, alternative fibers, supply-chain selection) and reduce feedstock water demands.

Material substitution trade-offs are evident: replacing PLA with a lower-carbon polymer might reduce GWP but could increase land use or water use depending on feedstock—careful multi-criteria assessment is essential.

4. Conclusion

The aim of this research is to conduct a comprehensive thermo-rheological and mechanical investigation of PLA-based biocomposites reinforced with hemp fibers and modified with polyethylene glycol (PEG). The variation of shear viscosity as a function of temperature and shear rate reveals a temperature-dependent pseudoplastic behavior. In addition, the chemical composition and intermolecular interactions of the PLA/Hemp/PEG system were analyzed using FTIR spectroscopy.

Subsequently, the 3D printing process was optimized using a design of experiments approach. Sets of printed plates were produced to evaluate the influence of nozzle temperature, printing speed, and layer thickness on part quality, with particular attention to surface finish and porosity. The experimental design identified optimal printing parameters of a nozzle temperature of 200 °C, a printing speed of 35 mm/s, and a layer thickness of 0.5 mm. Mechanical characterization of the printed parts was then performed through tensile testing to determine the mechanical properties of the PLA/Hemp/PEG biocomposites. The obtained strain stress curve for PLA-hemp and PLA/Hemp/PEG are typical of natural-fiber-reinforced polymers with quasi-brittle progressive tensile failure. The FTIR results are consistent with the tensile behavior, as the evolution of hydroxyl and ester bands with processing temperature indicates interfacial degradation and reduced fiber–matrix adhesion, which promotes progressive quasi-brittle failure under tensile loading. Finally, an LCA was conducted to evaluate the environmental impact of the biocomposites, considering each constituent material across six levels of analysis.

As a future perspective, numerical simulations of the 3D printing process will be developed by incorporating the experimentally determined rheological parameters into finite element modeling software (COMSOL Multiphysics), enabling predictive optimization of PLA/Hemp/PEG printed components.

Author Contributions:

Faleh RABHI, Ndeye Fatim NIANG, Liam CLOEZ, Mehdi BELHANI, Thierry BARRIERE and Mohamed SAHLI conceptualized the experiments and developed the methodology.

Faleh RABH, Ndeye Fatim NIANG and Liam CLOEZ performed the experiments and carried out the investigation. All authors contributed to the formal analysis.

Mehdi BELHANI performed the life cycle analysis of biocomposites.

Thierry BARRIERE and Mohamed SAHLI supervised the work. All authors contributed to the validation of the results. They also worked on the visualization and layout of the paper.

The original draft was primarily written by Faleh RABHI, and all authors contributed to review and editing.

Acknowledgments:

The authors would like to thank the UMLP (University of Marie and Louis Pasteur) for their financial support for this work. Experimental tests were carried out with the platforms in the Department of Applied Mechanics of Femto-st institute (AMETISTE for mechanical characterization, MIFHYSTO for polymer forming process). This work was conducted in the framework of the EIPHI Graduate School (contract "ANR-17-EURE-0002").

Conflicts of Interest:

The authors declare no conflict of interest.

5. References

[1] Bourell DL. : Perspectives on additive manufacturing. Annual Review of Materials Research, 46(1), 1-18 (2016).

[2] Xu X, Pamela RM, Christine MM, Alvaro G, Fanny J, Abdul WB, Simon G. : Stereolithography (SLA) 3D printing of an antihypertensive polyprintlet: Case study of an unexpected photopolymer-drug reaction. Additive Manufacturing, 33, 101071 (2020). https://doi.org/10.1016/j.addma.2020.101071

[3] Abdulhameed O, Abdulrahman AA, Wadea A, Syed HM. : Additive manufacturing: Challenges, trends, and applications. Advances in Mechanical Engineering, 11(2), 1687814018822880 (2019). https://doi.org/10.1177/1687814018822880

[4] Wong, KV, Hernandez A. : A review of additive manufacturing. International Scholarly Research Notices, 2012(1), 208760 (2012). https://doi.org/10.5402/2012/208760

[5] Ugur D, Bahar G, Ulas Y, Melik D. : The role of additive manufacturing in the era of Industry 4.0. Procedia Manufacturing, 11, 545-554 (2017). https://doi.org/10.1016/j.promfg.2017.07.148

[6] Ian G, David R, Brent S, Amirmahyar K. : Additive Manufacturing Technologies. Springer, Vol. 17. (2021). https://doi.org/10.1007/978-3-030-56127-7

[7] Saad SA, Sabu J, Namita RC, Naba KD. : Additive manufacturing of polymer materials: Progress, promise and challenges. Polymers, 13(5), 753 (2021). https://doi.org/10.3390/polym13050753

[8] Bi X, Huang R. : 3D printing of natural fiber and composites: A state-of-the-art review. Materials & Design, 222, 111065 (2022). https://doi.org/10.1016/j.matdes.2022.111065

[9] Frazier WE. : Metal additive manufacturing: A review. Journal of Materials Engineering and Performance, 2014, 23: 1917-1928. https://doi.org/10.1007/s11665-014-0958-z

[10] Gibson I, David R, Brent S, Amirmahyar K. : Design for additive manufacturing. In: Additive Manufacturing Technologies. Springer, 555-607 (2021). https://doi.org/10.1007/978-3-030-56127-7_19

[11] Gibson I, David R, Brent S, Amirmahyar K. : Development of additive manufacturing technology. In: Additive Manufacturing Technologies. Springer, 23-51 (2021). https://doi.org/10.1007/978-3-030-56127-7_2

[12] Najmon JC, Raeisi S, Tovar A. : Review of additive manufacturing technologies and applications in the aerospace industry. In: Additive Manufacturing for the Aerospace Industry, 7-31 (2019). https://doi.org/10.1016/B978-0-12-814062-8.00002-9

[13] Bikas H, Stavropoulos P, Chryssolouris G. : Additive manufacturing methods and modelling approaches: A critical review. The International Journal of Advanced Manufacturing Technology, 83: 389-405 (2016). https://doi.org/10.1007/s00170-015-7576-2

[14] Tumbleston JR, David S, Ashley RJ, David K, Kai C, Robert P, Jason PR. : Continuous liquid interface production of 3D objects. Science, 347(6228): 1349–1352 (2015). https://doi.org/10.1126/science.aaa2397

[15] Wohlers TT, Tim C. : 3D printing and additive manufacturing state of the industry. Annual Worldwide Progress Report, Wohlers Associates, (2014).

[16] Mazurchevici AD, Nedelcu,D, Popa R. : Additive manufacturing of composite materials by FDM technology: A review. Indian journal of engineering & materials sciences, (2020). https://doi.org/10.56042/ijems.v27i2.45920

[17] Solomon IJ, Sevvel P, Gunasekaran J. : A review on the various processing parameters in FDM. Materials Today: Proceedings, 37, 509–514 (2021). https://doi.org/10.1016/j.matpr.2020.05.484

[18] Tamir TS, Gang X, Qihang F, Xisong D, Zhen S, Feiyue W. : A feedback-based print quality improving strategy for FDM 3D printing: An optimal design approach. The International Journal of Advanced Manufacturing Technology, 120(3–4), 2777–2791 (2022). https://doi.org/10.1007/s00170-021-08332-4

[19] Abdul Khalil HPS, Md. SH, Enih R, Azli NA, Saddon N, Davoudpoura Y, Nazrul Islam Md, Rudi D. The role of soil properties and its interaction towards quality plant fiber: A review. Renewable & Sustainable Energy Reviews, 43, 1006–1015 (2015). https://doi.org/10.1016/j.rser.2014.11.099

[20] Latif R, Saif W, Noor ZK, Arshad NS, Shyam LV, Zahid AK. : Surface treatments of plant fibers and their effects on mechanical properties of fiber-reinforced composites: A review. Journal of Reinforced Plastics and Composites, 38(1), 15–30 (2018). https://doi.org/10.1177/0731684418802022

[21] Campilho RDSG Natural Fiber Composites. CRC Press, 368 (2015). https://doi.org/10.1201/b19062

[22] Faruk O, Andrzej KB, Hans-Peter F, Mohini S. : Biocomposites reinforced with natural fibers: 2000–2010. Progress in Polymer Science, 37(11), 1552–1596 (2012). https://doi.org/10.1016/j.progpolymsci.2012.04.003

[23] Madsen B, Gamstedt EK. : Wood versus plant fibers: similarities and differences in composite applications. Advances in Materials Science and Engineering, 2013: 564346 (2013). https://doi.org/10.1155/2013/564346

[24] Rana AK, Mandal A, Bandyopadhyay S. : Short jute fiber reinforced polypropylene composites: Effect of compatibiliser, impact modifier and fiber loading. Composites Science and Technology, 63(6), 801–806 (2003). http://dx.doi.org/10.1016/S0266-3538(02)00267-1

[25] Wang X, Jiang M, Zhou Z, Gou J, Hui D. : 3D printing of polymer matrix composites: A review prospective. Composites Part B: Engineering 110, 442–458 (2017). https://doi.org/10.1016/j.compositesb.2016.11.034

[26] Muthe LP, Pickering K, Gauss C. : A Review of 3D/4D Printing of Poly-Lactic Acid Composites with Bio-Derived Reinforcements. Composites Part C: Open Access 8, 100271 (2022). https://doi.org/10.1016/j.jcomc.2022.100271

[27] Salunkhe S, Murali A, Hussein MAM, Naranje V, Shanmugam R.. 3D printing of plant fiber reinforced polymer composites (PFRC's): an insight into methods, challenges and opportunities. Polymer-Plastics Technology and Materials, 62, 816-838 (2022). https://doi.org/10.1080/25740881.2022.2133612

[28] Li Y, Li Q. : Physical Properties of Plant Fiber Reinforced Composites. Engineering Materials. Springer, 143–175 (2022). https://doi.org/10.1007/978-981-19-5162-6_6

[29] Celiktas MS, Uyan M. : Plant fiber reinforced biocomposite: properties and applications. Mugla Journal of Science and Technology, 5, 42–48 (2019). https://doi.org/10.22531/muglajsci.566251

[30] Zhongsen Z, Shenming C, Yan L, Zhen W, Yu L, Tao Y, Yiou S,. High performances of plant fiber reinforced composites—A new insight from hierarchical microstructures. Composites Science and Technology, 194, 108151 (2020). https://doi.org/10.1016/j.compscitech.2020.108151

[31] Ramesh M, Palanikumar K, Reddy KH. : Plant fibre based bio-composites: Sustainable and renewable green materials. Renewable and Sustainable Energy Reviews, 79, 558–584 (2017). https://doi.org/10.1016/j.rser.2017.05.094

[32] Manaia JR, Ana TM, Lucia R. :. Industrial Hemp Fibers: An Overview. Fibers, 7(12), 106 (2019). https://doi.org/10.3390/fib7120106

[33] Pervaiz M, Panthapulakkal S, Kc B, Sain M, Tjong J. : Emerging Trends in Automotive Lightweighting through Novel Composite Materials. Materials Sciences and Applications, 7, 26–38 (2016). https://doi.org/10.4236/msa.2016.71004

[34] Joshi SV, Drzal LT, Mohanty AK, Arora S. :. Are natural fiber composites environmentally superior to glass fiber reinforced composites? Composites Part A: Applied Science and Manufacturing, 35(3), 371–376 (2004). https://doi.org/10.1016/j.compositesa.2003.09.016

[35] Witthayolankowit K, Rakkijakan T, Ayub R, Kumaniaev I, Pourchet S, Boni G, Watjanatepin P, Zarafshani H, Gabrion X, Chevallier A, Vo N, Van VA, Balaguer P, Van AK, Samec JSM, Placet V. : Use of a fully biobased and non-reprotoxic epoxy polymer and woven hemp fabric to prepare

environmentally friendly composite materials with excellent physical properties. Composites Part B: Engineering 258, 110692 (2023). https://doi.org/10.1016/j.compositesb.2023.110692

[36] Valbiom. : Panorama des fibres végétales en Europe et en Wallonie (2021).

[37] Guillaume C, Anaële L, Antoine LD, Alain B, Gilles A, Thierry G, Christophe B. : Effect of flax fibres individualisation on tensile failure of flax/epoxy unidirectional composite. Composites Part A: Applied Science and Manufacturing, 51, 62–70 (2013). https://doi.org/10.1016/j.compositesa.2013.03.018.

[38] Le D, Masahito U, David C, Ryosuke M, Mickaël C. : A review of 3D and 4D printing of natural fibre biocomposites. Materials & Design, 194, 108911 (2020). https://doi.org/10.1016/j.matdes.2020.108911.

[39] Muthe LP, Pickering K, Gauss C. : A Review of 3D/4D Printing of Poly-Lactic Acid Composites with Bio-Derived Reinforcements. Composites Part C: Open Access 8, 100271 (2022). https://doi.org/10.1016/j.jcomc.2022.100271.

[40] Gauss C, Pickering KL, Muthe LP. : The use of cellulose in bio-derived formulations for 3D/4D printing: A review. Composites Part C: Open Access 4, 100113 (2021). https://doi.org/10.1016/j.jcomc.2021.100113.

[41] Milosevic M, Stoof D, Pickering K. : Characterizing the mechanical properties of fused deposition modelling natural fiber recycled polypropylene composites. Journal of Composites Science, 1(1), 7 (2017). https://doi.org/10.3390/jcs1010007

[42] Coppola B, Emilia G, Luciano DM. : Investigation on the use of PLA/hemp composites for the fused deposition modelling (FDM) 3D printing. AIP Conference Proceedings, 1981, 020086 (2018). https://doi.org/10.1063/1.5045948

[43] Sawpan MA, Pickering KL, Fernyhough A. : Effect of fibre treatments on interfacial shear strength of hemp fibre reinforced polylactide and unsaturated polyester composites. Composites Part A: Applied Science and Manufacturing, 42, 1189–1196 (2011). https://doi.org/10.1016/j.compositesa.2011.05.003

[44] Aliotta L, Cinelli P, Coltelli MB, Righetti MC, Gazzano M, Lazzeri A. : Effect of nucleating agents on crystallinity and properties of poly (lactic acid) (PLA). European Polymer Journal 93, 822–832 (2017). https://doi.org/10.1016/j.eurpolymj.2017.04.041.

[45] Dai JX, Yang Q, Liu BJ. : Crystallization Behavior of PLA/PEG/Nucleating Agent Blends. Advanced Materials Research, 807–809, 578–581 (2013). https://doi.org/10.4028/www.scientific.net/AMR.807-809.578

[46] Tang Z, Zhang C, Liu X, Zhu J. : The crystallization behavior and mechanical properties of polylactic acid in the presence of a crystal nucleating agent. Journal of Applied Polymer Science 125, 1108–1115 (2012). https://doi.org/10.1002/app.34799.

[47] Ahmad SM, Pickering K, Fernyhough A. : Characterisation of hemp fibre reinforced poly(lactic acid). International Journal of Materials and Product Technology 36, 229–240 (2009).

[48] Delphine D, Michiel B, Kevin H, Wim S, Eleonora F, Frederik D, Jan I, Aart WVV,. Production and characterization of bamboo and flax fiber reinforced polylactic acid filaments for fused deposition modeling (FDM). Polymer Composites, 40, 1951-1963 (2018). https://doi.org/10.1002/pc.24971.

[49] David S, Kim LP, Yuanji Z. : Fused Deposition Modelling of Natural Fibre/Polylactic Acid Composites, 1(1), 8 (2017). https://doi.org/10.3390/jcs1010008

[50] George J, Ishida H. : A review on the very high nanofiller-content nanocomposites: Their preparation methods and properties with high aspect ratio fillers. Progress in Polymer Science, 86, 1–39 (2018). https://doi.org/10.1016/j.progpolymsci.2018.07.006

[51] Moudood A, Rahman A, Öchsner A, Islam M, Francucci G. :. Flax fiber and its composites: An overview of water and moisture absorption impact on their performance. Journal of Reinforced Plastics and Composites, 38, 323–339 (2019). https://doi.org/10.1177/0731684418818893.

[52] Charles DK, Frédéric D, Adam P, Antoine LD, Fabrizio S. The Design of 4D-Printed Hygromorphs: State-of-the-Art and Future Challenges. Advanced Functional Materials, 33, 2210353 (2023). https://doi.org/10.1002/adfm.202210353

[53] Mohammed M, Jawad AJM, Mohammed AM, Oleiwi JK, Adam T, Osman AF, Dahham OS, Betar BO, Gopinath SCB, Jaafar M. : Challenges and advancement in water absorption of natural fiber-reinforced polymer composites. Polymer Testing, 124, 108083 (2023). https://doi.org/10.1016/j.polymertesting.2023.108083.

[54] Bi X, Huang R. : 3D printing of natural fiber and composites: A state-of-the-art review. Materials & Design, 222, 111065 (2022). https://doi.org/10.1016/j.matdes.2022.111065.

[55] Kim YJ, Hong SJ, Shin WS, Kwon YR, Lim SH, Kim JS, Choi J, Kim JW, Kim DH. : Preparation and Performance of Superabsorbent Polymer with Cellulose Additives. Fibers Polym 21, 2448–2455 (2020). https://doi.org/10.1007/s12221-020-1198-5.

[56] Lamm ME, Wang L, Kishore V, Tekinalp H, Kunc V, Wang J, Gardner DJ, Ozcan S. : Material Extrusion Additive Manufacturing of Wood and Lignocellulosic Filled Composites. Polymers 12, 2115 (2020). https://doi.org/10.3390/polym12092115.

[57] Rakesh P, Singh I. : Processing of Green Composites (2019). https://doi.org/10.1007/978-981-13-6019-0

[58] Yu N, Sun X, Wang Z, Zhang D, Li J. : Effects of auxiliary heat on the interlayer bonds and mechanical performance of polylactide manufactured through fused deposition modeling. Polymer Testing, 104, 107390 (2021). https://doi.org/10.1016/j.polymertesting.2021.107390

[59] Pokharel A, Falua KJ, Babaei GA, Acharya B. : Biobased Polymer Composites: A Review. Journal of Composites Science, 6(9), 255 (2022). https://doi.org/10.3390/jcs6090255.

[60] Bianchi I, Forcellese A, Gentili S, Greco L, Simoncini M. : Comparison between the mechanical properties and environmental impacts of 3D printed synthetic and bio-based composites. Procedia CIRP, 105, 380–5 (2022). https://doi.org/10.1016/j.procir.2022.02.063.

[61] Ilyas RA, Sapuan SM, Harussani MM, Hakimi MYAY, Haziq MZM, Atikah MSN. : Polylactic Acid (PLA) Biocomposite: Processing, Additive Manufacturing and Advanced Applications. Polymers, 13, 1326 (2021). https://doi.org/10.3390/polym13081326.

[62] Momeni S, Safder M, Khondoker MAH, Elias AL. : Valorization of Hemp Hurds as Bio-Sourced Additives in PLA-Based Biocomposites. Polymers, 13, 3786 (2021). https://doi.org/10.3390/polym13213786.

[63] Yang S, Ma K, Liu Z, Ren J, Man Y. : Chapter 5 - Development and applicability of life cycle impact assessment methodologies. Life Cycle Sustainability Assessment for Decision-Making, 95–124 (2020). https://doi.org/10.1016/B978-0-12-818355-7.00005-1

[64] Muralikrishna IV, Manickam V. : Chapter Five - Life Cycle Assessment. Environmental Management, 57–75 (2017). https://doi.org/10.1016/B978-0-12-811989-1.00005-1.

[65] Hervy M, Evangelisti S, Lettieri P, Lee KY. : Life cycle assessment of nanocellulose-reinforced advanced fibre composites. Composites Science and Technology, 118, 154–62 (2015). https://doi.org/10.1016/j.compscitech.2015.08.024.

[66] Kumar R, Sharma H, Saran C, Tripathy TS, Sangwan KS, Herrmann C. A Comparative Study on the Life Cycle Assessment of a 3D Printed Product with PLA, ABS & PETG Materials. Procedia CIRP, 107, 15–20 (2022). https://doi.org/10.1016/j.procir.2022.04.003.

[67] Enarevba DR, Haapala KR. A Comparative Life Cycle Assessment of Expanded Polystyrene and Mycelium Packaging Box Inserts. Procedia CIRP, 116, 654–9 (2023). https://doi.org/10.1016/j.procir.2023.02.110.

Rheological, mechanical and life cycle assessment of 3D-printed PLA/Hemp/PEG biocomposites

Faleh Rabhi [a*], Ndeye Fatim Niang [a], Liam Cloëz [a], Thierry Barriere [a], Mehdi Belhani [b], Mohamed Sahli [c]

[a] Université Marie et Louis Pasteur, CNRS, Institut FEMTO-ST, Besançon, F-25000, France

[b] National Higher School of Technology and Engineering, L3M, 23005, Annaba, Algeria

[c] Centre de recherche sur les Ions, les Matériaux et la Photonique, Université Caen Normandie, ENSICAEN, CNRS, CEA, Normandie Univ, CIMAP UMR6252, F-14000 CAEN

***Corresponding author**

Email address: faleh.rabhi@femto-st.fr

Abstract

There is considerable interest in the development of bio-based materials for pellet-based material extrusion 3D printing as sustainable alternatives to conventional polymer composites. This study investigates Poly(Lactic Acid) (PLA) biocomposites reinforced with 20 wt% short Hemp fibers and modified with 5 wt% Polyethylene Glycol (PEG) as an additive. The rheological behavior of the biocomposite melts was analyzed using the Carreau–Yasuda model at different temperatures. Chemical behavior was evaluated through rheological tests coupled with fast-scan Fourier transform infrared (FTIR) spectroscopy conducted at 190 °C, 200 °C, and 210 °C. A design of experiments approach was employed to optimize the 3D printing parameters and to assess the influence of extrusion temperature, printing speed, and layer thickness on print quality. The optimal printing conditions for Hemp-based parts were identified as a temperature of 200 °C, a printing speed of 35 mm/s, and 0.5 mm of layer thickness. Mechanical testing was performed to evaluate the effect of Hemp fiber reinforcement on the performance of PLA-based printed parts, revealing a significant influence of Hemp fibers on the mechanical properties. In addition, a Life Cycle Assessment (LCA) was conducted to quantify the environmental impact of the PLA/Hemp/PEG. The results demonstrate that these materials represent a promising eco-friendly solution for sustainable additive manufacturing applications.

Highlights:

- Sustainable bio-based pellet-extrusion 3D printing is demonstrated
- Processing temperature effects on rheology and chemistry are analyzed
- Optimal printing conditions are 200 °C, 35 mm/s, and 0.5 mm layer thickness
- Hemp fibers significantly affect PLA mechanical properties
- LCA confirms the environmental benefits of PLA/Hemp/PEG composites.

Keywords: Biocomposite, Biopolymer, Natural Fiber, Rheology, Mechanical Properties, Additive Manufacturing.

~~Glossary~~

~~AM: Additive Manufacturing~~

~~FU: Functional Unit~~

~~FTIR: Fourier Transform Infrared Spectroscopy~~

~~FDM: Fused Deposition Modeling~~

~~H: Hemp~~

~~LCA: Life Cycle Assessment~~

~~PEG: Polyethylene Glycols~~

~~PFRCs: Plant Fiber-Reinforced Composites~~

~~PLA: Polylactic Acid~~

~~SQI: Soil Quality Index~~

Nomenclature

T_m	Melting temperature (°C)
a	Transition factor
n	Pseudo plasticity index
Pc	Porosity (%)
P_{wt}	Printed weight (kg)
T	Temperature (°C)
T_{wt}	Theoretical weight (kg)
V	Volume (m^3)
η_0	Zero-shear rate viscosity (Pa s)
η_∞	Infinite shear viscosity (Pa s)
λ	Characteristic time (s)
$\bar{\dot{\gamma}}$	Generalized shear rate (s^{-1})
ρ	Density (kg m^{-3})

1. Introduction

Additive Manufacturing (AM) began to emerge in the 1980s with the development of stereolithography [1, 2], which introduced the concept of building components layer by layer [3, 4]. Since then, AM has significantly reshaped conventional manufacturing process. It is now regarded as a valuable complement to conventional production methods, particularly well-suited for single-part fabrication, small-batch production, and the manufacturing of components with complex geometries, such as lattice structures [5, 6]. Moreover, the environmentally friendly and sustainable characteristics of AM have been key drivers of its rapid growth, as industries increasingly seek to reduce material waste and energy consumption [7, 8]. In recent years, the scope of AM applications has expanded steadily, especially in the automotive, medical, and aerospace industries [9–12]. A typical AM process involves several critical steps [13], including part design, data conversion, file transfer, printing preparation, and the layer-by-layer fabrication of the component using AM equipment until completion. Today, 3D printing is transitioning from a prototyping tool to a method for producing end-use parts. According to the Wohler's Report 2023, the global 3D printing industry reached $18 billion in 2022, with an annual growth rate of 18.3%. Its adoption continues to deepen across aerospace (16%), healthcare (14%), and automotive (12%). Advances in materials—such as metals, ceramics, and composites—and improvements in printing speed are expected to further strengthen its advantages and promote greater digitalization and flexibility within the manufacturing sector [14, 15]. Among AM technologies, Fused Deposition Modeling (FDM) is one of the most widely used solid-based processes. It enables the fabrication of three-dimensional components through the layer-by-layer deposition of thermoplastic materials. FDM has become one of the most accessible and cost-effective AM techniques, commonly used for rapid prototyping, functional component production, and materials research. Its versatility, ease of use, and ability to produce durable parts make it a preferred choice in aerospace, automotive, medical, and educational fields [16, 17]. The FDM process operates by extruding a continuous filament of thermoplastic material through a heated nozzle, which deposits the material along a predetermined toolpath to create successive layers [18]. Among the materials frequently utilized in FDM, Poly(Lactic Acid) (PLA) is widely favored due to its biodegradability, printability, and minimal warping tendency. However, its low thermal resistance (approximately 60 °C) and relatively brittle mechanical properties limit its use in high-performance applications.

In recent years, natural fiber-reinforced polymer composites (NFRPCs) have gained considerable attention as sustainable alternatives to conventional FDM materials. Plant fibers exhibit a broad range of physical and mechanical properties that are strongly influenced by their chemical composition, microstructural organization, and botanical origin. These characteristics determine their suitability for various applications, composite manufacturing, and biodegradable plastics. The principal physical and mechanical properties of plant fibers include density, moisture absorption, tensile strength, Young's modulus, elongation at break, and thermal stability [19, 20]. Biofibers have been widely employed as reinforcements and fillers in composite materials [21]. They originate from biological sources and are

generally classified into non-woody (natural) fibers and woody fibers [22]. Natural fibers often demonstrate superior physical and mechanical performance compared with woody fibers due to their higher cellulose content, greater crystallinity, and lower density [21]. Consequently, their industrial relevance has continued to increase [23]. Ideal attributes of natural fibers include high specific strength and modulus, good processing flexibility, low weight, low cost, and excellent resistance to corrosion and fatigue [24].

There has been growing interest in developing bio-composites that incorporate thermoplastics as matrices reinforced with various fillers, such as fibers, nanoparticles, and additives. Thermoplastic matrices offer several advantages, including ease of processing, recyclability, and the capability to form complex geometries through manufacturing techniques such as injection molding, compression molding, and additive manufacturing. Bio-sourced composites provide enhanced mechanical properties, improved durability, and reduced environmental impact relative to conventional materials [25]. Bio-derived reinforcements are generally classified as fibrous or particulate, depending on their morphology and size. Fibrous reinforcements can be further divided into discontinuous reinforcements—comprising individual fibers or chopped bundles forming short fibers—and continuous reinforcements, which consist of long continuous fibers spun into yarns [26].

Plant fiber-reinforced composites (PFRCs) incorporate plant-based fibers, such as hemp, as reinforcements within a polymer matrix [27]. These materials offer advantageous physical properties, including sound absorption, thermal insulation, and electromagnetic wave attenuation, making them attractive alternatives to synthetic fiber composites [28]. Nevertheless, PFRCs exhibit sensitivity to moisture and temperature variations, which can affect their performance and long-term durability [29]. Despite these limitations, PFRCs have demonstrated high potential in a wide range of applications, with properties such as fire resistance, acoustic behavior, and vibration damping being extensively investigated [30]. These composites have been extensively characterized through rheological, optical, mechanical, and thermo-mechanical analyses to assess their overall performance [29]. PFRCs exhibit notable mechanical properties, together with distinctive chemical compositions and hierarchical structural arrangements [28]. Nevertheless, a major limitation of PFRCs is the strong variability in their physical and mechanical characteristics [31], combined with their pronounced sensitivity to moisture and their complex, often nonlinear, mechanical behavior. A key advantage of plant-based fibers over synthetic fibers lies in their low density. Most plant fibers are considerably lighter than common synthetic reinforcements such as glass fibers, with the exception of carbon fibers. For instance, hemp fibers have a density of approximately 1.4 g/cm³, compared with 2.5 g/cm³ for glass fibers [32], while carbon fibers typically range between 1.4 and 1.7 g/cm³. This inherent lightness significantly reduces the mass of final composite components—an important benefit for the automotive industry, where lighter vehicles improve fuel efficiency and reduce greenhouse gas emissions. Consequently, the use of plant fibers in automotive parts contributes directly to lower CO_2 emissions [33]. When plant fibers are combined with biodegradable matrices such as PLA, the resulting composites offer enhanced

biodegradability and recyclability compared with synthetic fiber composites, thereby reducing environmental impact at end of life [34]. Moreover, the production of plant fibers requires substantially less energy than that of synthetic fibers. Hemp and flax fibers require about 5 MJ/kg and 9.5 MJ/kg, respectively, whereas glass fiber production demands around 57.4 MJ/kg [34, 35]. In addition, plant fibers such as hemp and flax can be cultivated locally, supporting regional economic development and promoting sustainable agricultural practices [36]. From a mechanical standpoint, although the properties of plant-fiber composites vary across plant species and fiber grades, they generally remain inferior to those of synthetic fiber composites at equivalent reinforcement contents. Coroller [37] demonstrated that for injection-molded composites containing 30 wt.% short fibers, glass fibers provide significantly higher Young's modulus and tensile strength than plant fibers such as hemp, flax, bamboo, and sisal. This difference is further amplified by the optimized surface treatments applied to synthetic fibers, which enhance fiber–matrix adhesion and improve interfacial load transfer. AM, or 3D printing, is increasingly transforming the fabrication of thermoplastic composites, including those reinforced with plant fibers. This layer-by-layer process, driven by a digital model, offers unprecedented flexibility in design and customization. For plant-fiber-reinforced composites, AM involves extruding a thermoplastic filament loaded with natural fibers through a heated nozzle and depositing the material sequentially to form the final structure. This approach enables the creation of complex geometries with minimal material waste. However, to fully exploit the potential of these materials, challenges related to print resolution, fiber orientation control, and post-processing requirements must be addressed [38]. With the increasing demand for sustainable and high-performance materials, the integration of NFRPCs with AM technologies has attracted growing interest. This combination offers a promising route for producing lightweight, biodegradable, and customizable components, enabling the fabrication of complex geometries while maintaining environmentally responsible characteristics. Among AM techniques, FDM and extrusion-based 3D printing have become particularly relevant for processing NFRPCs, where natural fibers such as hemp are blended with thermoplastics like PLA to create filament or pellet-based feedstocks. However, 3D printing natural fiber composites presents several challenges. Mechanical performance can be compromised by defects such as residual stresses, uneven fiber distribution, and insufficient fiber-to-matrix bonding [39]. Additional factors include the choice of fiber type, volume fraction, and interfacial adhesion, all of which strongly influence composite properties [40]. As highlighted by Le Duigou [38], the moderate mechanical performance of printed parts is often linked to the low fiber aspect ratio required for extrusion through narrow nozzles, which limits effective load transfer and results in weaker composite structures. M. Milosevic et al. [41] demonstrated significant improvements in mechanical properties when 30 wt.% hemp or harakeke fibers were incorporated into polypropylene, reporting increases in tensile strength and Young's modulus of more than 50% and 143%, respectively. Similarly, B. Coppola et al. [42] observed that the incorporation of hemp powder into PLA reduced melt viscosity during compounding, influencing printability. Due to the short fiber lengths typically used in FDM, controlling fiber orientation remains critical for maintaining deposition quality. The microstructure and composition of plant fibers are also key determinants of

mechanical performance, with fiber surface properties strongly affecting interfacial adhesion and stress transfer. Poor fiber–matrix bonding in FDM-printed composites frequently leads to extrusion-related defects such as porosity, which in turn reduce stiffness and strength. Chemical surface treatments, including alkali, acetic anhydride, maleic anhydride, and silane treatments, have been shown to enhance interfacial adhesion. Sawpan et al. [43] reported increased interfacial shear strength for most treated PLA/hemp systems—up to 11.4 MPa for alkali-treated fibers—and even higher values in UPE/hemp composites, reaching 20.3 MPa for fibers treated with combined Na-OH and silane. Defect minimization is therefore essential, as defects such as porosity and delamination substantially degrade mechanical properties. Strategies to reduce porosity include vacuum drying of fibers, strict control of printing humidity and temperature, and the use of plasticizers such as PEG, although PEG contents above 10 wt.% can reduce tensile strength [44–46]. Fiber content also plays a critical role: Sawpan et al. [47] found that increasing hemp fiber content from 0 to 30 wt.% in PLA composites enhanced tensile strength and Young's modulus, and substantially increased flexural modulus. Impact strength improved up to 20 wt.% but deteriorated at higher contents due to increased porosity and reduced interfacial bonding [48]. Fiber loadings above 20 wt.% may also cause excessive melt viscosity, resulting in non-uniform extrusion and poor interlayer adhesion [49]. Fiber aspect ratio further influences reinforcement efficiency. Low aspect ratios limit load transfer and may cause debonding rather than effective stress transmission [38], whereas higher aspect ratios enhance mechanical performance [50]. However, aspect ratio selection is constrained by nozzle diameter, as long fibers can cause clogging and dispersion issues. Moisture management is another critical factor. Plant fibers and some bio-based polymers such as PLA are moisture-sensitive, which can lead to printing defects and material degradation. As reported for flax fibers [51], moisture uptake weakens the fiber–matrix interface and compromises composite quality. Kariz et al. showed that increasing moisture content (33–87%) reduced the stiffness of wood/PLA composites. Moisture present during processing may vaporize, generating porosity and adhesion problems [52], altering crystallinity [53], and creating internal stresses that cause warping [38]. During service, moisture sensitivity can impair dimensional stability and damage the fiber–matrix interface [54, 55]. Therefore, rigorous drying and conditioning prior to processing are essential [56, 57]. Finally, local pre-deposition heating has been shown to enhance interlayer adhesion in FDM-printed PLA. Yu et al. [58] demonstrated that such auxiliary heating improved tensile strength from 38.4 MPa to 63.6 MPa and reduced mechanical anisotropy from 0.51 to 0.22, reflecting a substantial improvement in structural integrity.

PLA is recognized as an environmentally friendly material due to its versatility, as it can be recycled, incinerated, composted, or safely landfilled. Its production also requires 25–55% less energy than conventional polymers, reinforcing its sustainability [59]. Natural fibers such as flax, hemp, jute, kenaf, and ramie are commonly used in AM filaments [60, 61, 62]. When combined with PLA, these fibers create fully renewable filaments, enhancing the environmental performance of additive manufacturing.

Chemically treated fibers further improve functional properties, supporting sustainable material development in both academia and industry.

Life Cycle Assessment (LCA) is a standard method for evaluating the environmental impacts of products or processes [63, 64]. Cradle-to-grave LCA examines the full life cycle, while gate-to-gate or gate-to-grave focus on production-to-use or production-to-disposal impacts. The methodology involves four steps: goal and scope definition, inventory analysis, impact assessment, and result interpretation [64]. Specialized software, with comprehensive material and process databases, is often used to streamline calculations.

Hemp-based filaments have lower environmental impacts than synthetic alternatives, particularly for Cumulative Energy Demand, Global Warming Potential, and Abiotic Depletion Potential, making them a sustainable alternative to glass fiber-reinforced polymers [60, 65]. Comparative LCAs using tools like Umberto NXT and SimaPro, along with databases such as ecoinvent and methods like ReCiPe, CML, or IMPACT 2002+, show that raw material extraction dominates PLA's environmental footprint, notably in freshwater ecotoxicity and water depletion [60, 66, 67].

The present study investigates the thermo-rheological and mechanical behavior of PLA-based biocomposites. The compositional and chemical structure of the PLA/Hemp/PEG system was characterized using Fourier-transform infrared spectroscopy (FTIR). Subsequently, the 3D printing process was optimized through a design of experiments approach, producing sets of printed plates to evaluate the influence of nozzle temperature, printing speed, and layer thickness on surface quality and porosity. Mechanical characterization of the printed parts was performed via tensile testing to assess the mechanical performance of PLA/Hemp/PEG. Finally, an LCA was conducted to evaluate the environmental impact of the biocomposites, considering six levels of component-specific analysis.

2. Materials and methods

This section focuses on descriptions of the materials used in 3D printing and the various characterization methods.

2.1. Materials

2.1.1. ~~Description of PLA~~ Properties of PLA

PLA (PLI 005) is a specialized PLA pellet grade designed for a variety of thermoplastic manufacturing processes. It is provided by Natureplast (Mondeville, France), a company specializing in bioplastics. PLA exists in several isomeric forms, mainly PLLA (poly-L-lactic acid) and PDLA (poly-D-lactic acid). PLA PLI 005 is primarily made of PLLA, which has a semicrystalline structure that offers the mechanical strength and stability required for injection molding and blow molding applications. Table 1 summarizes the properties of PLA PLI 005.

Table 1: properties and characteristics of PLA PLI 005

Property	Value
Bio-based content	100 %
Density	1.25 g/cm^3
MFI	25- 35 g/10 min
Melting temperature (T_m)	169 – 179 °C
Tensile modulus	3500 MPa
Elongation at break	4 %

2.1.2. ~~Description of the PLA /Hemp/PEG composites~~ Properties of the PLA/Hemp/PEG composites

Hemp fibers are natural materials obtained from the Cannabis sativa plant. They are long, strong, and durable, with fiber bundles ranging from a few centimeters up to several tens of centimeters. Hemp fibers are valued for their tensile strength, light weight, and environmentally friendly cultivation, which typically requires minimal or no pesticides.

The PLA/Hemp composite retained in this work was provided by Automotive Performance Materials (Dijon, France). It is produced on an industrial line designed for large-scale manufacturing of composite pellets, featuring a twin-screw extruder with multiple dosing units and a granulator to ensure uniform quality. This facility delivers ready-to-use blends for automotive applications, using regionally sourced agricultural fibers. The matrix material is PLA, reinforced with 20 wt% short hemp fibers.

The PLA–Hemp pellets initially supplied by APM contained 30 wt% hemp without additives, which led to poor extrudability and unstable flow during printing. In order to obtain a formulation suitable for P-

MEX, the fibre content was reduced to 20 wt% and several additives were screened (different PEG molecular weights and stearic acid) to facilitate mixing extrusion and printing processes. Internally, PEG content was varied from 0 to 10 wt% in 2.5 wt% increments, but rheological shear curves largely overlapped, indicating only limited additional benefit beyond 5 wt% in terms of viscosity reduction and flow behavior. This is consistent with literature showing that PEG improves PLA processability but that higher PEG contents can detrimentally affect mechanical performance and morphology by excessive plasticization or phase separation. A PEG content of 5 wt% was therefore selected as a compromise: sufficient to ease extrusion and printing of the 20 wt% hemp composite, while limiting the risk of degradation of mechanical properties. On this basis, the objective of the present work was to optimize processing parameters for this reference formulation, rather than to perform a full optimization of PEG content.

Polyethylene Glycols (PEG) from Merck KGaA (Allemagne) is chosen as plasticizer for composite formulations. PEG 1500 improves process ability and flexibility with its moderate molecular weight. This material ensures uniform dispersion and facilitate the extrusion and molding process, optimizing mechanical properties. The properties of PEG are shown in Table 2.

The binder was formulated using 75 wt% PLA PLI 5 and 20 wt% Hemp and 5 wt% additive.

Table 2: PEG description and properties

Additive	Density (g/cm^3)	Tm (°C)
PEG 1500	1.2	43 - 49

2.2. Methods

2.2.1. Rheological behavior of PLA/Hemp/PEG biocomposites

A comprehensive series of rheological tests was conducted to fit the experimental data to the Carreau-Yasuda model. The shear viscosity of molten PLA/Hemp (above its melting temperature) was measured using a rotational cone-and-plate rheometer over both low and high shear rates, within a temperature range of 190 - 210 °C. For PLA/Hemp/PEG, measurements were performed at shear rates from 1 to 500 s^{-1} to evaluate the effect of shear rate on viscosity. Each test was repeated three times to ensure reproducibility.

Rheological characterization was carried out with a Thermo Fisher Scientific HAAKE MARS III rotational rheometer (Thermo Fisher Scientific, Illkirch-Graffenstaden, France) in oscillatory dynamic (frequency sweep) mode, using a cone-and-plate setup with a 2° angle. The biocomposite sample was placed between a stationary disk and a coaxial cone of equal radius. The cone was rotated around the shared axis at a controlled angular velocity, while the sample on the lower disk was gradually positioned to the required gap. All tests were replicated three times to guarantee consistent and reproducible results. The rheological model involved in the Carreau-Yasuda law is represented by Eq. (1):

$$\eta = \eta_\infty + (\eta_0 - \eta_\infty)\left(1 + \left(\lambda\dot{\bar{\gamma}}\right)^a\right)^{\frac{n-1}{a}} \quad (1)$$

where $\eta_0$is the zero-shear rate viscosity, λ is the characteristic Newtonian-to-pseudoplastic transition time of the polymer, the parameter a reflects the transition curvature between the Newtonian plateau and the decreasing asymptote of the power law, n is the pseudo-plasticity index and $\dot{\bar{\gamma}}$ is the generalized shear rate.

2.2.2. Manufacturing processes

In this study, the COGIT printer was employed to print structures in PLA/Hemp/PEG, Figure 1. The COGIT 3D printer (COGIT Composites, France) is a high-precision additive manufacturing system capable of producing complex geometries directly from digital designs. It offers excellent reproducibility and supports a variety of materials for both prototyping and functional uses. With its integrated hardware and software optimizations, the printer ensures accurate layer deposition, structural consistency, and reliable operation, making it a versatile tool for research, engineering, and experimental applications in additive manufacturing.

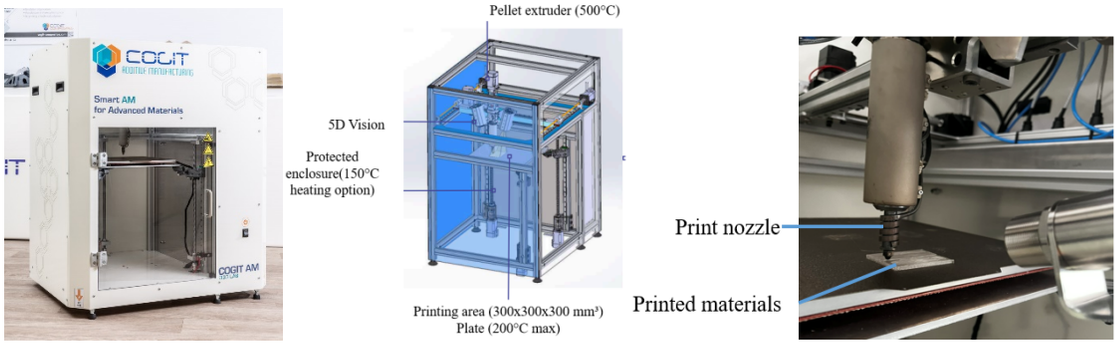

Figure 1: COGIT AM's 3D printer.

The technical and thermal properties of the equipment used are detailed in Table 3.

Tableau 3: Technical Specifications of the 3D Printer.

Parameters	**Fused Granular Fabrication**
Material packaging	Granules or Filaments
Print volume	300 x 300 x 300 mm³
Maximum extrusion temperature	500 °C
Maximum temperature of the plate	200 °C
Maximum number of extruders	1
Maximum print speed	100 mm/s
Movement accuracy	X, Y : 10 µm / Z : 2µm
Layer thickness	Mini 100 µm
Nozzle size	From 0.4 to 1.2 mm
Dimensions (L x W x H)	800 x 700 x 1050 mm³

2.2.3. Printing optimization methodology

To optimize 3D printing parameters involving three factors, each at three levels, the L9 Taguchi orthogonal array is used. This array offers an efficient and balanced approach to evaluate the effects of each factor individually and in combination with others. Orthogonal experiments are a structured experimental design widely used in engineering, statistics, and manufacturing. Their main purpose is to identify which factors most significantly influence a specific response. This is achieved by systematically varying the factors in a controlled manner to maintain orthogonality while reducing the total number of experiments. Each factor is tested at the same number of levels, and the initial optimization focuses on minimizing the adverse effects of porosity.

The porosity (Pc) of the sample, which indicates the percentage of voids or pores within the material, is calculated using the Eq. (2). To accurately assess the properties of the 3D-printed sample, the procedure begins by measuring its actual weight using a precise analytical scale, which provides the printed weight, denoted as P_{wt}:

$$P_c(\%) = \left(1 - \frac{P_{wt}}{T_{wt}}\right) \times 100 \quad (2)$$

The theoretical weight (T_{wt}) of the sample is then calculated using the formula $T_{wt} = V \times \rho$. This theoretical weight represents the weight the sample would have if it were free of any internal voids or pores.

2.2.4. Rheology coupled to fast-scan FTIR spectroscopy

FTIR combined with rheology enables real-time monitoring of the kinetic evolution of reactive systems. Integrating both techniques in a single instrument allows the rheological behavior to be directly correlated with molecular-scale structural changes, particularly the vibrations of functional groups in chemical bonds. The FTIR spectrometer operates at high acquisition speeds, capturing the onset of reactions simultaneously with rheological measurements. This setup, known as RHEONAUT, combines a Thermo Scientific Haake MARS III rheometer (Thermo Fisher Scientific, Illkirch-Graffenstaden, France) with a 20 mm parallel-plate geometry featuring a transparent window, and a Nicolet IS10 FTIR spectrophotometer equipped with a specialized acquisition system. Mid-infrared spectra (400–4000 cm^{-1}) were recorded at a resolution of 4 cm^{-1}, with each spectrum representing 32 scans. The module uses a single-reflection diamond ATR (attenuated total reflection) optical unit with an integrated electrical heater, enabling studies of molten polymers up to 400 °C. Infrared radiation passes through the crystal to the sample interface, where it is partially absorbed and reflected, then redirected to the detector using mirrors and lenses for precise measurement.

2.2.5. Mechanical characterization

Tensile testing was carried out at room temperature using an MTS Criterion Model 45 universal testing machine (MTS Systems Corporation, Créteil, France) fitted with a 5 kN load cell and contact extensometers. A constant crosshead speed of 2 mm/min was applied. The specimens, designed

according to ISO 527-4 type 1B geometry (Figure 2), were laser-cut from printed parallelepiped samples to ensure high dimensional precision and smooth surfaces suitable for transverse extensometer measurements. The mean values of Young's modulus, tensile strength, and fracture strain were obtained in accordance with the ISO 527 standard, with Young's modulus evaluated over a strain interval ranging from 0.05 % to 0.25 % (Figure 3).

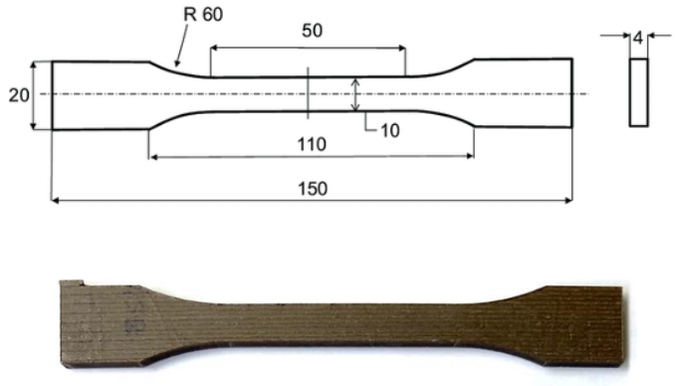

Figure 2: ISO 527-4 type 1B sample dimensions

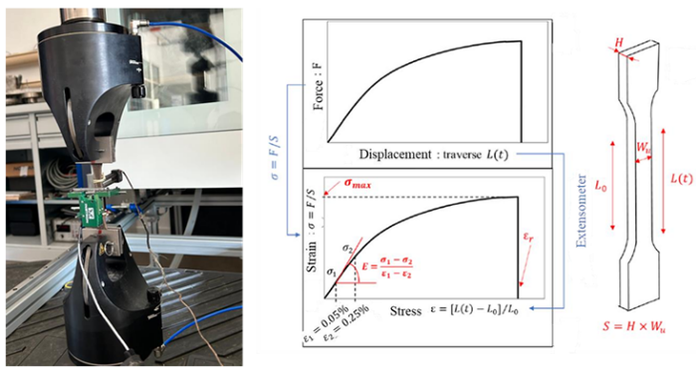

Figure 3: MTS machine testing and tensile methodology

2.2.6. Life cycle assessment of PLA/Hemp/PEG

LCA is a systematic method used to evaluate the environmental impacts of a product, process, or service throughout its entire life cycle. It considers all stages, from raw material extraction to production, use, and end-of-life. LCA helps identify opportunities to reduce environmental impacts and support sustainable decision-making.

The system boundaries take the creadle-to-gate with the production of PLA, Hemp fiber and composite. The Hemp fiber is modeled as flax fiber with the same production efficiency. The French mix is used to produce the hemp fiber and the composite. The LCA is carried out with the use of OpenLCA software 2.3.1 and Ecoivent v3.5 and the environmental impacts are calculated with EF 3.0.

3. Results and discussions

3.1. Rheology and identification

The measures of shear viscosity as a function of the shear rate and temperature are displayed in Figure 4. The curves clearly exhibit a thermo-dependent pseudoplastic behavior since viscosity decreases as a function of temperature and shear rate.

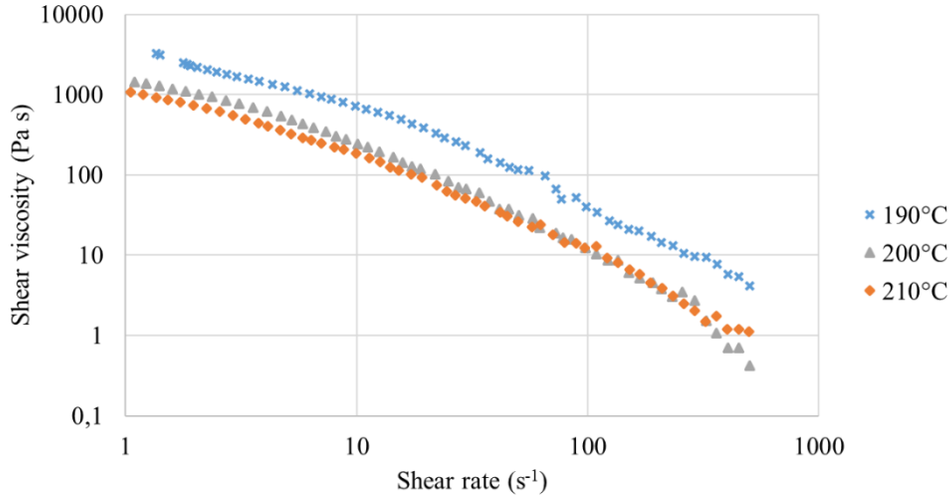

Figure 4: Experimental shear viscosity of PLA/Hemp/PEG versus shear rate and temperature.

The values of the identified parameters were obtained by the least square method with the MATLAB software using the experimental data and are summarized in Table 4:

The value n < 1 confirms the pseudoplastic behavior of the PLA/Hemp composite. $\eta\infty$ was set null at high shear rate according to the observed vanishing viscosity. As temperature increases, $\eta 0$ and λ decrease, while n and a slightly increase, according to usual time temperature correspondence between the interaction time and temperature involving a time scaling and temperature scaling equivalence in shear viscosity, relaxation time, and conservation modulus curves.

Table 4: Carreau-Yasuda model parameters identified for PLA/Hemp/PEG composites.

T **(°C)**	η_0 **(Pa s)**	η_∞	λ **(s)**	***n***	***a***
190	3000	0	0.25	0.35	2
200	1500	0	0.125	0.45	2.2
210	900	0	0.06	0.50	2.5

3.2. Optimization of printing process

Producing dense parts from different formulations requires thorough optimization of printing parameters. Key factors affecting print quality include nozzle and bed temperature, nozzle diameter, and printing speed. Nozzle temperature primarily influences the material's viscosity, while printing speed controls the extrusion flow rate. Among these, nozzle temperature, layer height, and printing speed are critical, whereas other parameters have a smaller impact and can be fixed. Optimization of these

parameters was conducted under the specific test conditions listed in Table 5, focusing on maximizing part density and ensuring geometric accuracy.

Table 5: Printing parameters for optimization of PLA/Hemp formulations

Levels	Nozzle Temperature (°C)	Layer Thickness (mm)	Printing Speed (mm/s)
1	190	0.3	30
2	200	0.4	40
3	210	0.5	50

The effects of three factors were explored at 3 levels each mainly, the printing temperature, the layer height and the printing speed, Figure 5. The infill is held at 100 % and the nozzle diameter selected is 1 mm with a bed temperature at 50 °C.

The L9 Taguchi design clearly identifies main effects: fiber content (dominant, 7 - 13 % porosity rise at 20 wt% due to fiber-induced voids); nozzle temperature (decrease in porosity due to better adhesion and stabilization close to 200 °C); layer height (positive correlation, thicker layers increase voids); printing speed (minor effect 30 - 50 mm/s). These align with literature on FDM porosity drivers.

Optimal settings (200 °C, intermediate layer height, 35 mm/s, 20 wt% fiber) minimize porosity by balancing melt flow for interlayer diffusion without fibre degradation. As a conclusion, L9 orthogonal arrays prioritize main effects over interactions, which are confounded and difficult to resolve reliably.

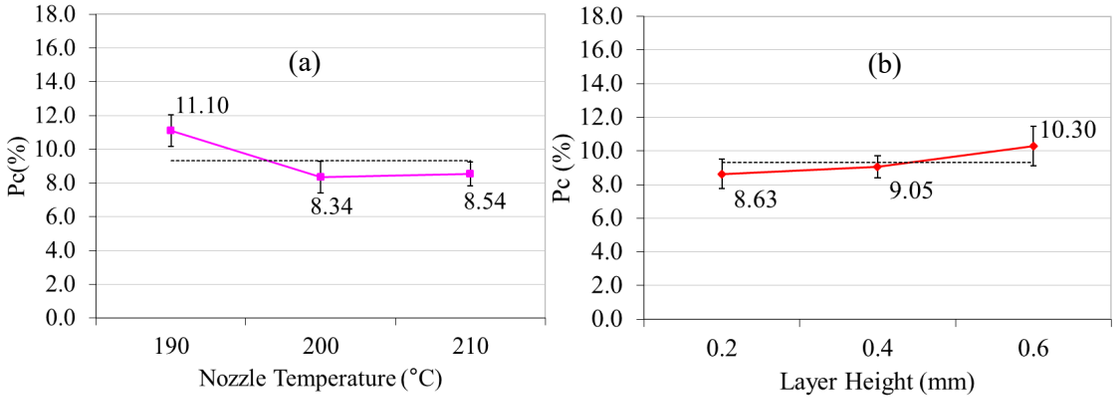

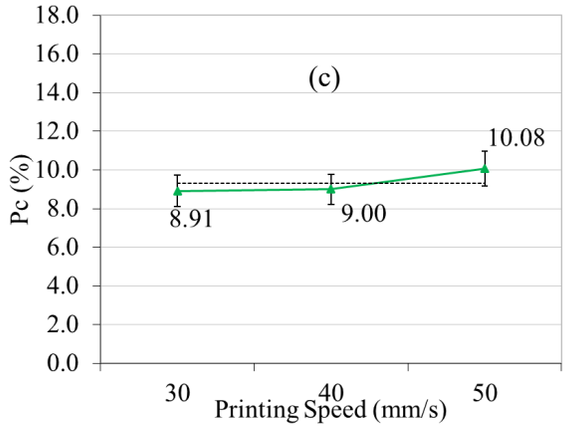

Figure 5: Effects of factors from DOE (Taguchi method) a) printing temperature, b) layer height and c) printing velocity.

Figure 5 (a) shows the influence of nozzle temperature on porosity. When the temperature is increased from 190 °C to 200 °C, porosity decreases from 11.10% to 8.34 %. Increasing the temperature further to 210 °C results in a slight rise in porosity to 8.54 %. The small difference between 200 °C and 210 °C indicates that the effect of nozzle temperature on porosity reduction may plateau or slightly reverse at higher temperatures. This behavior could be due to minor variations in thermal control during printing, causing small fluctuations in porosity. Overall, the most significant decrease in porosity occurs between 190 °C and 200 °C, highlighting this range as critical for improving layer consolidation.

Figure 5 (b) illustrates the relationship between layer height and porosity. Porosity increases from 8.63% to 10.30 % as the layer height is raised from 0.2 mm to 0.6 mm. This suggests that thicker layers may lead to higher porosity, potentially due to less accurate layer deposition and weaker interlayer bonding. While the error bars show some overlap, indicating measurement variability, the overall trend of increasing porosity with greater layer height remains consistent and should be considered when optimizing printing parameters.

Figure 5 (c) illustrates the effect of printing speed on porosity. Porosity remains approximately 9 % at speeds of 30 mm/s and 40 mm/s, with a slight increase to 10 % at 50 mm/s. This suggests that, within the tested range of 30 - 50 mm/s, printing speed has a relatively minor influence on porosity compared with factors such as fiber content or nozzle temperature. However, as the data are limited to three points and the variations are small, this trend should be interpreted cautiously. Overall, the impact of printing speed on porosity appears to be limited within this range.

The print settings employed in this study are shown in Table 6.

Table 6: Print parameters for PLA/Hemp/PEG

Layer height	0.5 mm
Fill rate	100 %
Fill pattern	Rectilinear

Upper heating zone temperature	190 °C
Middle heating zone temperature	195 °C
Nozzle temperature	200 °C
Bed temperature	50 °C
Print speed	35 mm/s

The influence of temperature on print quality is shown in Figure 6. With the same print speed and layer thickness, the sample printed at 200 °C has a higher surface quality than those printed at 190 °C and 210 °C. The raster angles of ± 45° were initially selected because they are widely used in literature as a reference orientation for evaluating the mechanical and process behavior of 3D-printed composites and polymers. This bidirectional pattern provides a balanced in-plane stress distribution and allows assessment of the material's performance under multi-directional loading. Using ± 45° orientations during the parameter optimization phase ensured that the process settings (layer height, flow rate, temperature, etc.) were not biased toward a single fiber or filament direction. Once the optimal parameters were identified, additional samples printed at 0° and 90° were tested to analyze the influence of orientation, with the 0° configuration showing superior properties.

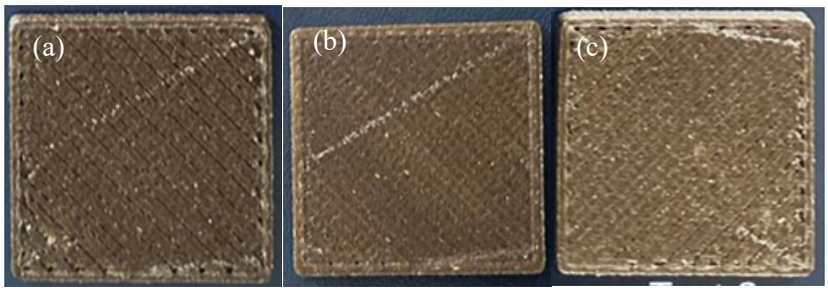

Figure 6: Printed samples in the extrusion temperature range of (a) 190 °C, (b) 200 °C and (c) 210 °C.

3.3. FTIR spectroscopy

The 3D printed PLA/Hemp/PEG biocomposites were subjected FTIR analysis to evaluate the chemical constituents at different temperatures (190 °C, 200 °C and 210 °C), Figure 7. Analysis of the results shows the presence of O-H bonds, it confirms the presence of the cellulose and hemicellulose which belongs to the hemp fibers.

C=O indicates the bonding between the PLA and hemp hydroxyl group depicting better interfacial compatibility between the constituents.

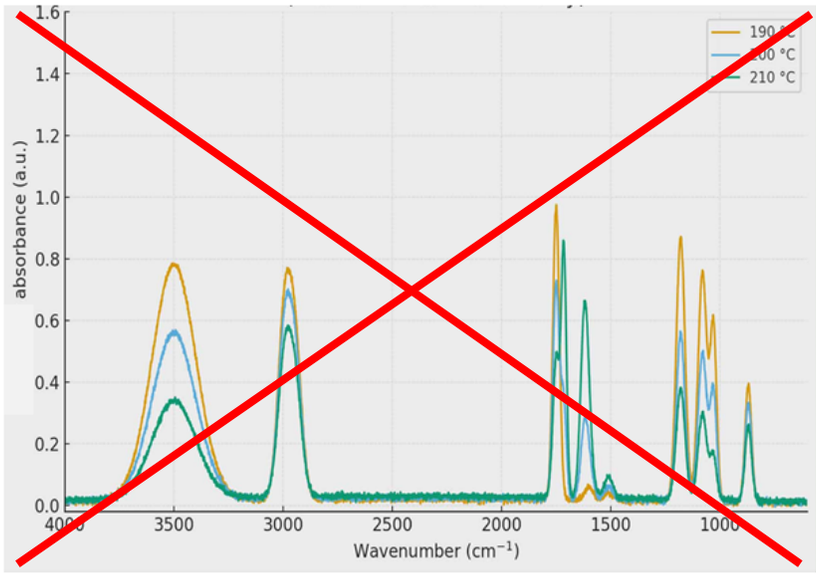

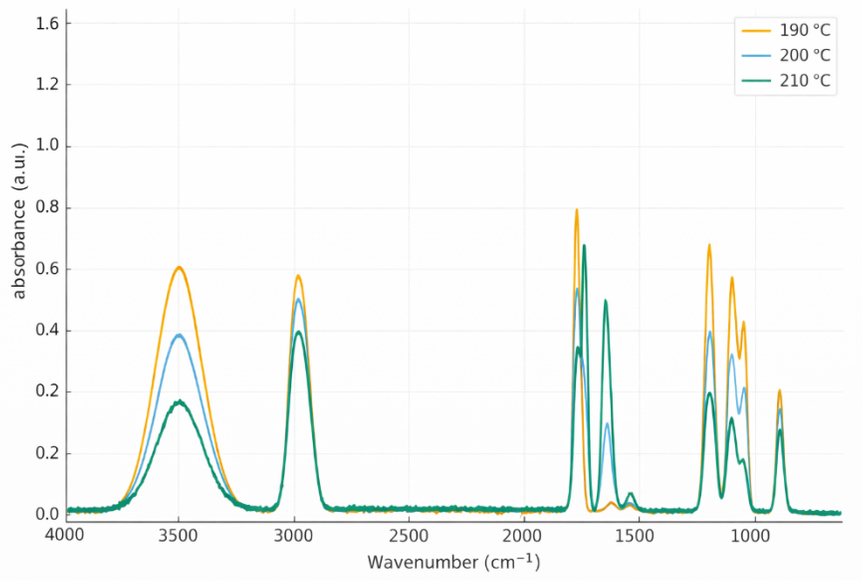

Figure 7: FTIR spectra of PLA/Hemp biocomposites at 190°C, 200°C and 210°C.

The FTIR spectra recorded at 190 °C, 200 °C, and 210 °C reveal progressive chemical modifications within the PLA/hemp biocomposite as temperature increases. A pronounced decrease of the broad O–H stretching band around 3500 cm^{-1} is observed, reflecting dehydration and the gradual degradation of hydroxyl-rich cellulose and hemicellulose in the hemp fibers. The aliphatic C–H stretching region between 3000–2850 cm^{-1} also diminishes steadily with temperature, indicating increasing scission of PLA chains, particularly those involving methyl substituents. The characteristic PLA ester carbonyl peak at ~1750 cm^{-1} shows a strong decline from 190 °C to 210 °C, confirming extensive chain cleavage, while a new peak around 1715 cm^{-1} grows in intensity, consistent with the formation of oxidized carbonyl species such as ketones, carboxylic acids, and terminal degradation products. Simultaneously, the absorption band near 1620 cm^{-1} becomes more pronounced at higher temperatures, likely arising from conjugated C=C structures formed during hemicellulose pyrolysis and partial transformation of lignin, as well as unsaturated degradation fragments. Additional temperature-dependent reductions in

the C–O–C and C–O stretching bands in the 1180–1080 cm^{-1} and ~1030 cm^{-1} regions reflect depolymerization of PLA and cleavage of polysaccharide glycosidic linkages. Finally, a noticeable elevation of the baseline at 210 °C—particularly in the lower wavenumber region—suggests the formation of char, thermally induced aromatic conjugation, and oxidation byproducts, collectively confirming advanced thermal degradation of both the polymer matrix and the natural fibers.

Table 7 shows the prominent spectral peaks, their chemical structure in the form of a functional group for PLA/Hemp biocomposites.

Table 7: Summary of FTIR Spectra for PLA/Hemp/PEG biocomposites (190 → 210 °C)

Wavenumber Region	Functional Group	Trend (190→210 °C)	Interpretation
~3500 cm^{-1}	OH	↓ strong decrease	dehydration + cellulose degradation
3000–2850 cm^{-1}	C–H	↓ slight/moderate	PLA chain scission
1750 cm^{-1}	C=O (PLA ester)	↓ significant	PLA depolymerization
1715 cm^{-1}	C=O (degradation)	↑	oxidized carbonyls (acids/ketones)
~1620 cm^{-1}	C=C	↑	conjugated and lignin-derived structures
1180–1080 / 1030	C–O–C / C–O	↓	degradation of PLA & polysaccharides
—	Baseline	↑	carbonaceous residue (char) formation

3.4. Mechanical behavior

The mechanical behavior of the PLA/Hemp composites under tensile loading is summarized in Figure 8. The strain stress curves corresponding to three repetitive tests for two materials (PLA-20H and and PLA-20H-PEG). This behavior is typical of natural-fiber-reinforced polymers with quasi-brittle progressive tensile failure. The mechanism is dominated by matrix cracking, interfacial debonding, and fiber pull-out. The tensile test results indicate that the addition of hemp (PLA-20H) and the combined incorporation of hemp with PEG (PLA-20H-PEG) slightly influence the mechanical properties of PLA. The tensile strength remains relatively constant across all samples, with PLA, PLA-20H, and PLA-20H-PEG exhibiting values around 40 MPa, suggest ting that the fillers do not significantly compromise the strength of the matrix.

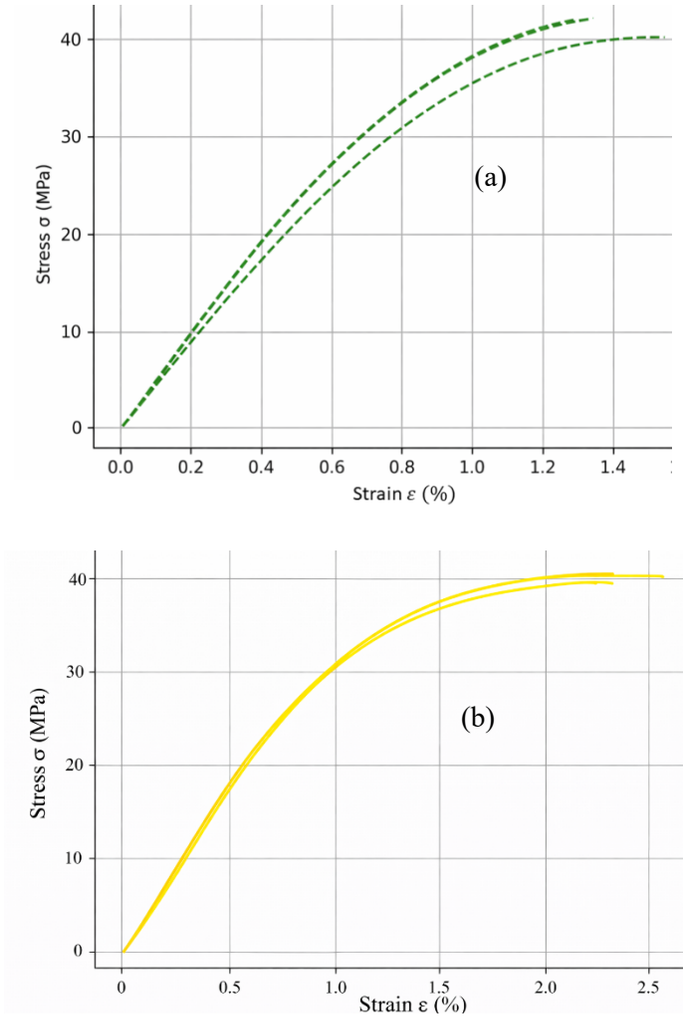

Figure 8: Influence of additives on the tensile properties of the pellet-based material extrusion of the formulations (a) PLA-20H and (b) PLA-20H-PEG.

In terms of stiffness, measured by Young's modulus, both PLA-20H and PLA-20H-PEG show a noticeable increase compared to neat PLA, indicating that the incorporation of hemp fibers enhances the rigidity of the composite. Specifically, Young's modulus increases from approximately 3.5 GPa for PLA to about 5 GPa for the modified composites, Figure 9.

Elongation at break demonstrates the most pronounced effect of PEG addition. While PLA and PLA-20H display similar ductility (~1.35%), the PLA-20H-PEG composite exhibits a higher elongation at break (~2.5%), indicating that PEG acts as a plasticizer, improving the flexibility of the material without compromising tensile strength.

As a conclusion, the results suggest that the PLA-20H-PEG composite achieves a balanced combination of strength, stiffness, and ductility, making it a promising material for applications requiring both mechanical performance and enhanced flexibility. The PLA–hemp composite exhibits a nonlinear tensile response with progressive damage characterized by matrix cracking, fiber–matrix debonding, and fiber pull-out, leading to quasi-brittle failure.

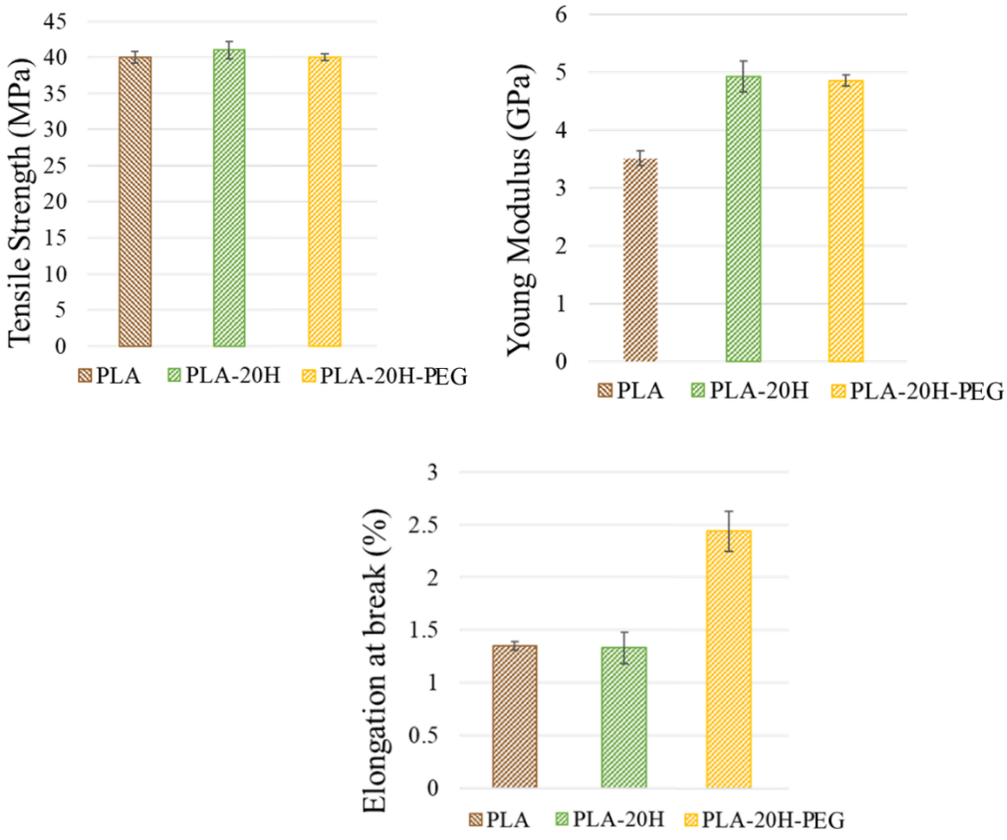

Figure 9: Tensile strength and Young's modulus values and Elongation at break of PLA, PLA-20H and PLA-20H-PEG.

The different mechanical properties of composites are presented in Table 8.

Table 8: Tensile properties of PLA, PLA-20H and PLA-20H-PEG

	PLA	PLA-20H	PLA-20H-PEG
E (GPa)	3.5 ± 0.50	4.9 ± 0.27	4.85 ± 0.10
σ (MPa)	40 ± 1	41 ± 1.17	40 ± 0.48
ε (%)	1.35 ± 0.15	1.3 ± 0.15	2.4 ± 0.19
ν	0.35 ± 0.02	0.38 ± 0.02	0.36 ± 0.02

3.5. LCA of PLA/Hemp: Contribution analysis by process/component (per kg)

The functional unit (FU) chosen for the LCA study is mass (kg). For one FU of material, the composition consists of 0.75 kg of PLA, 0.20 kg of hemp fiber, and 0.05 kg of plasticizer. In addition to the material inputs, the process requires an energy consumption of 99.900 kJ per FU.

Table 9 summarizes the environmental impacts of the composite material assessed using the EF 3.0 method and normalized per functional unit of composite mass. The climate change impact, expressed as

GWP100, is 5.18 kg CO_2 equivalent. The depletion of energy resources (ADP) amounts to 364.07 MJ. Acidification potential is estimated at 0.034 mol H^+ equivalent, while photochemical oxidation reaches 0.020 kg NMVOC equivalent. Water use associated with the functional unit is 11.22 m^3, and land use, expressed by the Soil Quality Index (SQI), is 92.40.

Table 9: The environmental impacts with EF 3.0 method

	FU per composite mass (kg)
Climate change GWP100 (kg CO2eq)	5.18
Energy resources ADP (MJ)	364.07
Acidification AE (mol H+ eq)	0.034
Photochemical oxidation (kg NMVOC eq)	0.020
Water use (m^3)	11.22
Land use SQI (-)	92.40

Table 10 summarizes the percentage contribution of four system elements—~~3D printing (process)~~ PLA/Hemp/PEG composites, PLA (polymer matrix), hemp fiber, and PEG (additive)—to six environmental impact categories on a per-kilogram basis. Figures 9–14 show the component contributions for each impact category, and Figure 15 presents a stacked comparison across all categories.

Table 10: The contribution processes in the environmental impacts (%): per kg

	~~3D printing~~ PLA/Hemp/PEG composites	PLA	Hemp fiber	PEG
Climate change GWP100 (kg CO_2-eq)	48.29	46.47	3.21	2.04
Energy resources -ADP (MJ)	91.13	7.8	0.37	0.7
Acidification AE (mol H+ eq)	49.69	44.04	4.94	1.32
Photochemical oxidation (kg NMVOC eq)	45.70	47.76	4.91	1.73
Water use (m^3)	35.94	40.57	23.13	0.36
Land use SQI (-)	17.92	28.01	53.86	0.21

The contributions to global warming potential (GWP100), Figure 10, are dominated by ~~3D printing (process)~~ printing PLA/Hemp/PEG composites ~~3D printing process~~ (48.29 %) and PLA production (46.47 %), with hemp fiber and PEG together contributing only ~5.3 %. This indicates that emissions related to electricity or thermal energy use during printing and the cradle-to-gate emissions of PLA (feedstock cultivation, fermentation, and polymerization) are the principal drivers of the carbon footprint

for the studied composite. Any mitigation strategy aiming at GWP reduction should therefore first target machine energy consumption (e.g., energy-efficient printing, process optimization, or low-carbon electricity) and secondarily raw material selection or low-GWP PLA supply chains.

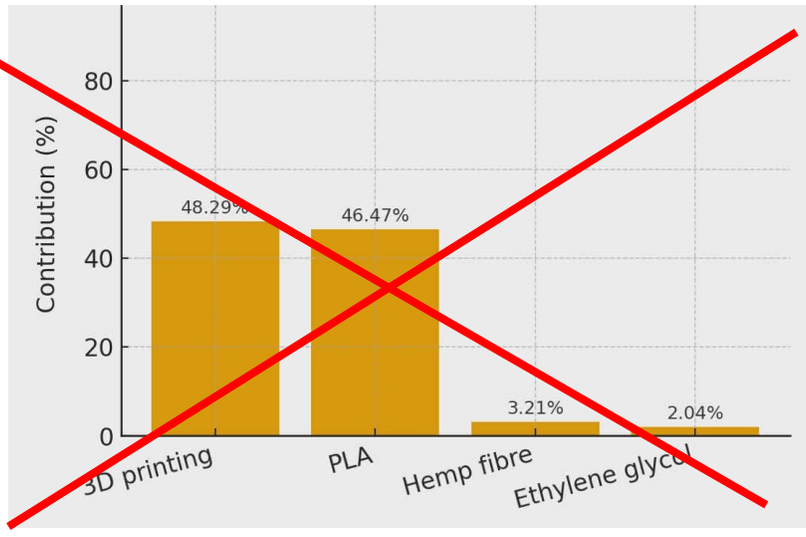

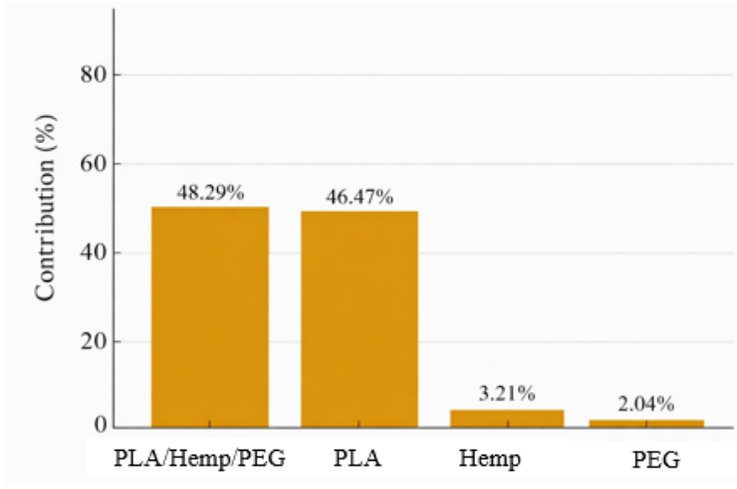

Figure 10: Contribution to climate change GWP100 (Kg CO_2eq)

Energy-resource depletion is overwhelmingly attributed to printing PLA/Hemp/PEG composites ~~the printing process~~ (91.13 %), while PLA accounts for only 7.8 % and the other components are negligible, Figure 11. This shows that the operation-phase (electricity, heating) of the printer is by far the most energy-intensive stage for a kilogram of printed composite. Reducing printing energy per mass (e.g., higher deposition rates, batch printing, and optimized process parameters) or switching to renewable electricity would substantially lower the ADP indicator.

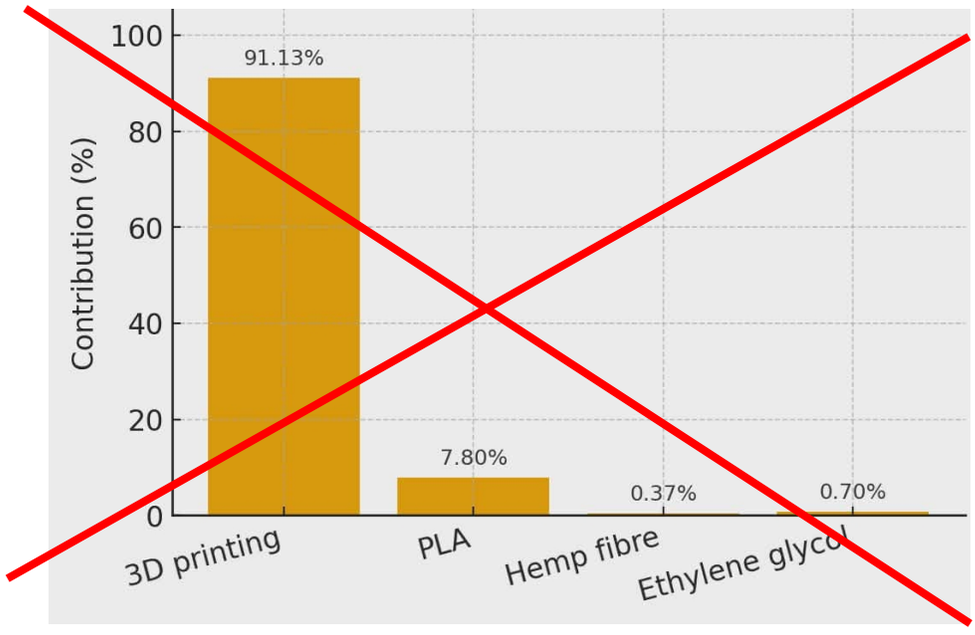

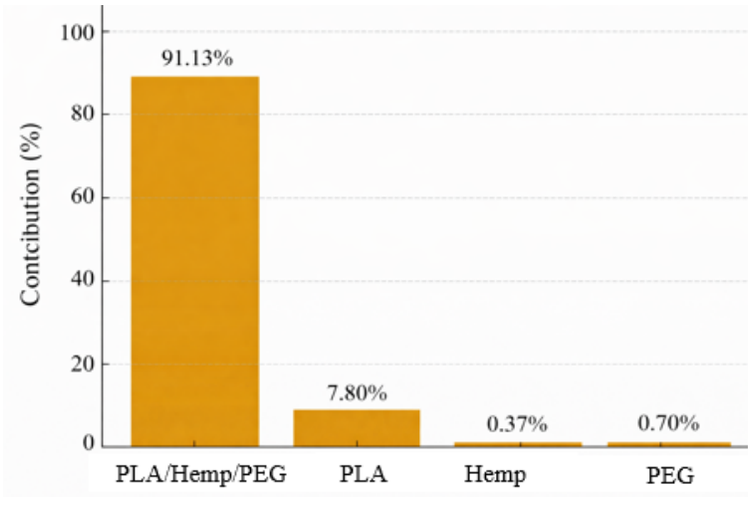

Figure 11: Contribution to energy resources - ADP (MJ)

Acidification potential is split primarily between printing PLA/Hemp/PEG composites ~~3D printing~~ (49.69 %) and PLA (44.04 %), mirroring the pattern observed for climate change. These contributions likely stem from fossil-fuel combustion and industrial emissions in both energy supply and PLA production pathways (e.g., fertilizer use or combustion emissions during feedstock processing). Targeted emission controls in feedstock cultivation and energy production could therefore reduce acidifying emissions.

Photochemical oxidation (precursor emissions for tropospheric ozone) is almost evenly split between PLA (47.76 %) and 3D printing (45.70 %), with hemp fiber and ethylene glycol minor. The significant role of PLA suggests that volatile organic compound emissions during feedstock processing or polymer manufacturing contribute meaningfully to smog formation potential.

Water consumption differs from the previously discussed categories: PLA (40.57 %) and printing PLA/Hemp/PEG composites ~~3D printing~~ (35.94 %) are both significant, but hemp fiber accounts for a

notable 23.13 %, Figure 12. This reflects agricultural water needs in hemp cultivation as well as water used in PLA feedstock (e.g., irrigation in biomass production). For water-limited regions, material sourcing (choice of feedstock, irrigation practices) and process water management are crucial.

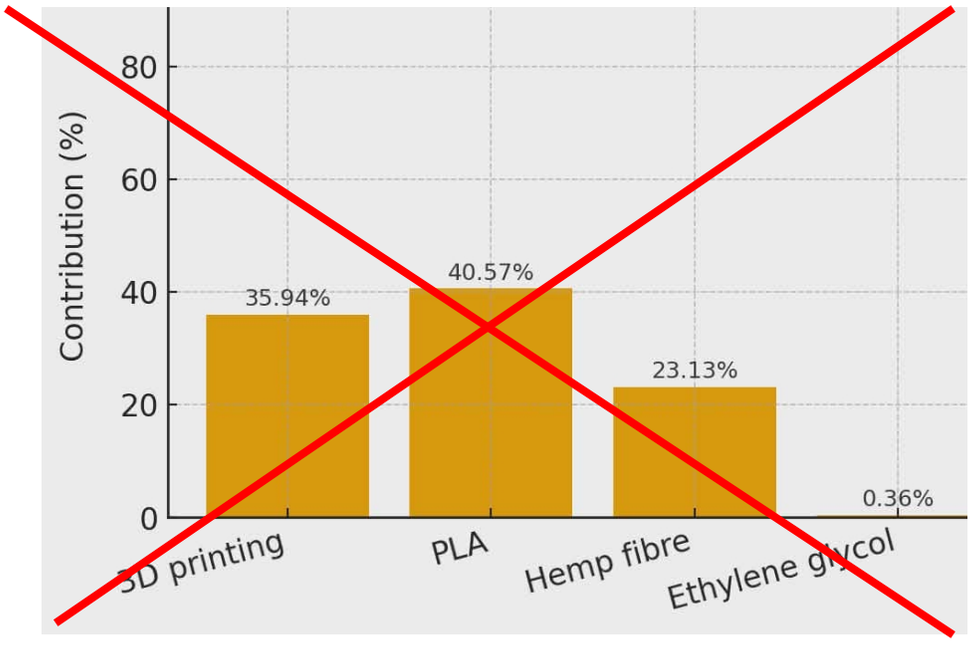

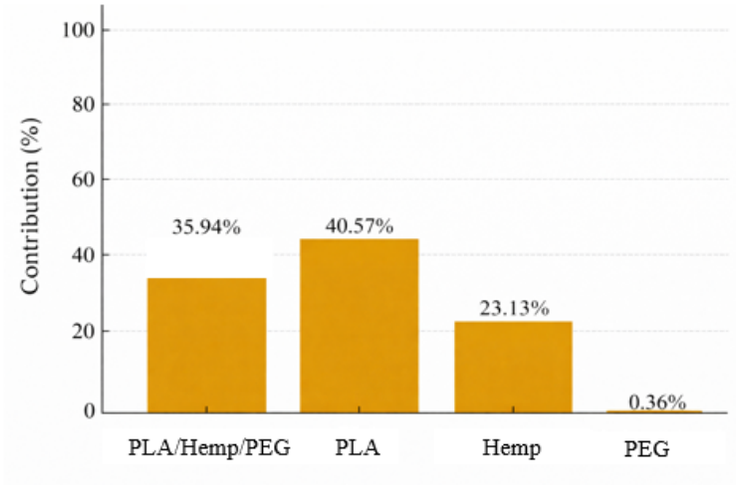

Figure 12: Contribution to water use (m^3)

The hemp fiber dominates land use (53.86 %), followed by PLA (28.01 %) and printing PLA/Hemp/PEG composites ~~printing process~~ (17.92 %). This strong dominance of hemp in land occupation arises from the agricultural land required for fiber production. If land-use minimization is a priority (biodiversity or food-land competition concerns), strategies may include using agricultural residues, higher-yield fiber crops, or sourcing hemp from low-impact land types.

~~The~~ Printing PLA/Hemp/PEG composites ~~3D printing process~~ is the single largest contributor to energy-related impacts and is a major contributor for climate, acidification, and photochemical oxidation. PLA is consistently a major contributor across most impact categories, particularly climate, photochemical oxidation, water use, and land use. Hemp fiber contributes disproportionately to land use and

significantly to water use, but negligibly to energy and climate categories. PEG has only minor contributions across all categories for this system.

If the objective is to lower GWP and ADP simultaneously, prioritize interventions on the printing of PLA/Hemp/PEG composites ~~process~~ (energy use reduction, machine efficiency, renewable electricity). If the objective targets land and water footprint, focus on fiber sourcing (agricultural practice improvements, alternative fibers, supply-chain selection) and reduce feedstock water demands.

Material substitution trade-offs are evident: replacing PLA with a lower-carbon polymer might reduce GWP but could increase land use or water use depending on feedstock—careful multi-criteria assessment is essential.

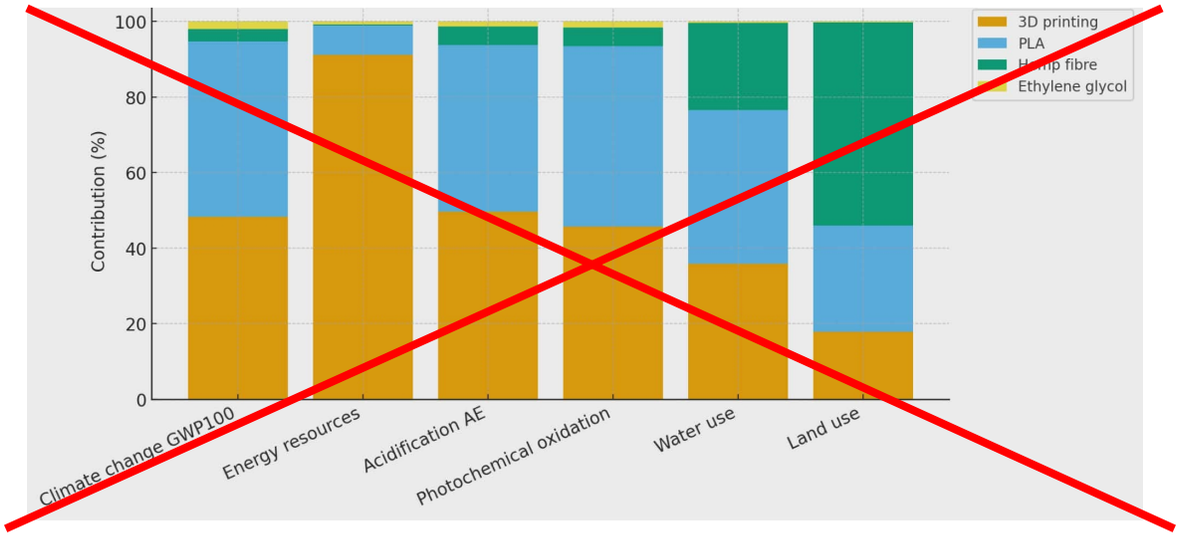

~~Figure 13: Stacked contributions by component across impact categories (per kg)~~

4. Conclusion

The aim of this research is to conduct a comprehensive thermo-rheological and mechanical investigation of PLA-based biocomposites reinforced with hemp fibers and modified with polyethylene glycol (PEG). The variation of shear viscosity as a function of temperature and shear rate reveals a temperature-dependent pseudoplastic behavior. In addition, the chemical composition and intermolecular interactions of the PLA/Hemp/PEG system were analyzed using FTIR spectroscopy.

Subsequently, the 3D printing process was optimized using a design of experiments approach. Sets of printed plates were produced to evaluate the influence of nozzle temperature, printing speed, and layer thickness on part quality, with particular attention to surface finish and porosity. The experimental design identified optimal printing parameters of a nozzle temperature of 200 °C, a printing speed of 35 mm/s, and a layer thickness of 0.5 mm. Mechanical characterization of the printed parts was then performed through tensile testing to determine the mechanical properties of the PLA/Hemp/PEG biocomposites. The obtained strain stress curve for PLA-hemp and PLA/Hemp/PEG are typical of natural-fiber-reinforced polymers with quasi-brittle progressive tensile failure. The FTIR results are consistent with the tensile behavior, as the evolution of hydroxyl and ester bands with processing temperature indicates interfacial degradation and reduced fiber–matrix adhesion, which promotes progressive quasi-brittle failure under tensile loading. Finally, a LCA was conducted to evaluate the environmental impact of the biocomposites, considering each constituent material across six levels of analysis.

As a future perspective, numerical simulations of the 3D printing process will be developed by incorporating the experimentally determined rheological parameters into finite element modeling software (COMSOL Multiphysics), enabling predictive optimization of PLA/Hemp/PEG printed components.

Author Contributions:

Faleh RABHI, Ndeye Fatim NIANG, Liam CLOEZ, Mehdi BELHANI, Thierry BARRIERE and Mohamed SAHLI conceptualized the experiments and developed the methodology.

Faleh RABH, Ndeye Fatim NIANG and Liam CLOEZ performed the experiments and carried out the investigation. All authors contributed to the formal analysis.

Mehdi BELHANI performed the life cycle analysis of biocomposites.

Thierry BARRIERE and Mohamed SAHLI supervised the work. All authors contributed to the validation of the results. They also worked on the visualization and layout of the paper.

The original draft was primarily written by Faleh RABHI, and all authors contributed to review and editing.

Acknowledgments:

The authors would like to thank the UMLP (University of Marie and Louis Pasteur) for their financial support for this work. Experimental tests were carried out with the platforms in the Department of Applied Mechanics of Femto-st institute (AMETISTE for mechanical characterization, MIFHYSTO for polymer forming process). This work was conducted in the framework of the EIPHI Graduate School (contract "ANR-17-EURE-0002").

Conflicts of Interest:

The authors declare no conflict of interest.

5. References

[1] Bourell DL. : Perspectives on additive manufacturing. Annual Review of Materials Research, 46(1), 1-18 (2016).

[2] Xu X, Pamela RM, Christine MM, Alvaro G, Fanny J, Abdul WB, Simon G. : Stereolithography (SLA) 3D printing of an antihypertensive polyprintlet: Case study of an unexpected photopolymer-drug reaction. Additive Manufacturing, 33, 101071 (2020). https://doi.org/10.1016/j.addma.2020.101071

[3] Abdulhameed O, Abdulrahman AA, Wadea A, Syed HM. : Additive manufacturing: Challenges, trends, and applications. Advances in Mechanical Engineering, 11(2), 1687814018822880 (2019). https://doi.org/10.1177/1687814018822880

[4] Wong, KV, Hernandez A. : A review of additive manufacturing. International Scholarly Research Notices, 2012(1), 208760 (2012). https://doi.org/10.5402/2012/208760

[5] Ugur D, Bahar G, Ulas Y, Melik D. : The role of additive manufacturing in the era of Industry 4.0. Procedia Manufacturing, 11, 545-554 (2017). https://doi.org/10.1016/j.promfg.2017.07.148

[6] Ian G, David R, Brent S, Amirmahyar K. : Additive Manufacturing Technologies. Springer, Vol. 17. (2021). https://doi.org/10.1007/978-3-030-56127-7

[7] Saad SA, Sabu J, Namita RC, Naba KD. : Additive manufacturing of polymer materials: Progress, promise and challenges. Polymers, 13(5), 753 (2021). https://doi.org/10.3390/polym13050753

[8] Bi X, Huang R. : 3D printing of natural fiber and composites: A state-of-the-art review. Materials & Design, 222, 111065 (2022). https://doi.org/10.1016/j.matdes.2022.111065

[9] Frazier WE. : Metal additive manufacturing: A review. Journal of Materials Engineering and Performance, 2014, 23: 1917-1928. https://doi.org/10.1007/s11665-014-0958-z

[10] Gibson I, David R, Brent S, Amirmahyar K. : Design for additive manufacturing. In: Additive Manufacturing Technologies. Springer, 555-607 (2021). https://doi.org/10.1007/978-3-030-56127-7_19

[11] Gibson I, David R, Brent S, Amirmahyar K. : Development of additive manufacturing technology. In: Additive Manufacturing Technologies. Springer, 23-51 (2021). https://doi.org/10.1007/978-3-030-56127-7_2

[12] Najmon JC, Raeisi S, Tovar A. : Review of additive manufacturing technologies and applications in the aerospace industry. In: Additive Manufacturing for the Aerospace Industry, 7-31 (2019). https://doi.org/10.1016/B978-0-12-814062-8.00002-9

[13] Bikas H, Stavropoulos P, Chryssolouris G. : Additive manufacturing methods and modelling approaches: A critical review. The International Journal of Advanced Manufacturing Technology, 83: 389-405 (2016). https://doi.org/10.1007/s00170-015-7576-2

[14] Tumbleston JR, David S, Ashley RJ, David K, Kai C, Robert P, Jason PR. : Continuous liquid interface production of 3D objects. Science, 347(6228): 1349–1352 (2015). https://doi.org/10.1126/science.aaa2397

[15] Wohlers TT, Tim C. : 3D printing and additive manufacturing state of the industry. Annual Worldwide Progress Report, Wohlers Associates, (2014).

[16] Mazurchevici AD, Nedelcu,D, Popa R. : Additive manufacturing of composite materials by FDM technology: A review. Indian journal of engineering & materials sciences, (2020). https://doi.org/10.56042/ijems.v27i2.45920

[17] Solomon IJ, Sevvel P, Gunasekaran J. : A review on the various processing parameters in FDM. Materials Today: Proceedings, 37, 509–514 (2021). https://doi.org/10.1016/j.matpr.2020.05.484

[18] Tamir TS, Gang X, Qihang F, Xisong D, Zhen S, Feiyue W. : A feedback-based print quality improving strategy for FDM 3D printing: An optimal design approach. The International Journal of Advanced Manufacturing Technology, 120(3–4), 2777–2791 (2022). https://doi.org/10.1007/s00170-021-08332-4

[19] Abdul Khalil HPS, Md. SH, Enih R, Azli NA, Saddon N, Davoudpoura Y, Nazrul Islam Md, Rudi D. The role of soil properties and its interaction towards quality plant fiber: A review. Renewable & Sustainable Energy Reviews, 43, 1006–1015 (2015). https://doi.org/10.1016/j.rser.2014.11.099

[20] Latif R, Saif W, Noor ZK, Arshad NS, Shyam LV, Zahid AK. : Surface treatments of plant fibers and their effects on mechanical properties of fiber-reinforced composites: A review. Journal of Reinforced Plastics and Composites, 38(1), 15–30 (2018). https://doi.org/10.1177/0731684418802022

[21] Campilho RDSG Natural Fiber Composites. CRC Press, 368 (2015). https://doi.org/10.1201/b19062

[22] Faruk O, Andrzej KB, Hans-Peter F, Mohini S. : Biocomposites reinforced with natural fibers: 2000–2010. Progress in Polymer Science, 37(11), 1552–1596 (2012). https://doi.org/10.1016/j.progpolymsci.2012.04.003

[23] Madsen B, Gamstedt EK. : Wood versus plant fibers: similarities and differences in composite applications. Advances in Materials Science and Engineering, 2013: 564346 (2013). https://doi.org/10.1155/2013/564346

[24] Rana AK, Mandal A, Bandyopadhyay S. : Short jute fiber reinforced polypropylene composites: Effect of compatibiliser, impact modifier and fiber loading. Composites Science and Technology, 63(6), 801–806 (2003). http://dx.doi.org/10.1016/S0266-3538(02)00267-1

[25] Wang X, Jiang M, Zhou Z, Gou J, Hui D. : 3D printing of polymer matrix composites: A review prospective. Composites Part B: Engineering 110, 442–458 (2017). https://doi.org/10.1016/j.compositesb.2016.11.034

[26] Muthe LP, Pickering K, Gauss C. : A Review of 3D/4D Printing of Poly-Lactic Acid Composites with Bio-Derived Reinforcements. Composites Part C: Open Access 8, 100271 (2022). https://doi.org/10.1016/j.jcomc.2022.100271

[27] Salunkhe S, Murali A, Hussein MAM, Naranje V, Shanmugam R.. 3D printing of plant fiber reinforced polymer composites (PFRC's): an insight into methods, challenges and opportunities. Polymer-Plastics Technology and Materials, 62, 816-838 (2022). https://doi.org/10.1080/25740881.2022.2133612

[28] Li Y, Li Q. : Physical Properties of Plant Fiber Reinforced Composites. Engineering Materials. Springer, 143–175 (2022). https://doi.org/10.1007/978-981-19-5162-6_6

[29] Celiktas MS, Uyan M. : Plant fiber reinforced biocomposite: properties and applications. Mugla Journal of Science and Technology, 5, 42–48 (2019). https://doi.org/10.22531/muglajsci.566251

[30] Zhongsen Z, Shenming C, Yan L, Zhen W, Yu L, Tao Y, Yiou S,. High performances of plant fiber reinforced composites—A new insight from hierarchical microstructures. Composites Science and Technology, 194, 108151 (2020). https://doi.org/10.1016/j.compscitech.2020.108151

[31] Ramesh M, Palanikumar K, Reddy KH. : Plant fibre based bio-composites: Sustainable and renewable green materials. Renewable and Sustainable Energy Reviews, 79, 558–584 (2017). https://doi.org/10.1016/j.rser.2017.05.094

[32] Manaia JR, Ana TM, Lucia R. :. Industrial Hemp Fibers: An Overview. Fibers, 7(12), 106 (2019). https://doi.org/10.3390/fib7120106

[33] Pervaiz M, Panthapulakkal S, Kc B, Sain M, Tjong J. : Emerging Trends in Automotive Lightweighting through Novel Composite Materials. Materials Sciences and Applications, 7, 26–38 (2016). https://doi.org/10.4236/msa.2016.71004

[34] Joshi SV, Drzal LT, Mohanty AK, Arora S. :. Are natural fiber composites environmentally superior to glass fiber reinforced composites? Composites Part A: Applied Science and Manufacturing, 35(3), 371–376 (2004). https://doi.org/10.1016/j.compositesa.2003.09.016

[35] Witthayolankowit K, Rakkijakan T, Ayub R, Kumaniaev I, Pourchet S, Boni G, Watjanatepin P, Zarafshani H, Gabrion X, Chevallier A, Vo N, Van VA, Balaguer P, Van AK, Samec JSM, Placet V. : Use of a fully biobased and non-reprotoxic epoxy polymer and woven hemp fabric to prepare

environmentally friendly composite materials with excellent physical properties. Composites Part B: Engineering 258, 110692 (2023). https://doi.org/10.1016/j.compositesb.2023.110692

[36] Valbiom. : Panorama des fibres végétales en Europe et en Wallonie (2021).

[37] Guillaume C, Anaële L, Antoine LD, Alain B, Gilles A, Thierry G, Christophe B. : Effect of flax fibres individualisation on tensile failure of flax/epoxy unidirectional composite. Composites Part A: Applied Science and Manufacturing, 51, 62–70 (2013). https://doi.org/10.1016/j.compositesa.2013.03.018.

[38] Le D, Masahito U, David C, Ryosuke M, Mickaël C. : A review of 3D and 4D printing of natural fibre biocomposites. Materials & Design, 194, 108911 (2020). https://doi.org/10.1016/j.matdes.2020.108911.

[39] Muthe LP, Pickering K, Gauss C. : A Review of 3D/4D Printing of Poly-Lactic Acid Composites with Bio-Derived Reinforcements. Composites Part C: Open Access 8, 100271 (2022). https://doi.org/10.1016/j.jcomc.2022.100271.

[40] Gauss C, Pickering KL, Muthe LP. : The use of cellulose in bio-derived formulations for 3D/4D printing: A review. Composites Part C: Open Access 4, 100113 (2021). https://doi.org/10.1016/j.jcomc.2021.100113.

[41] Milosevic M, Stoof D, Pickering K. : Characterizing the mechanical properties of fused deposition modelling natural fiber recycled polypropylene composites. Journal of Composites Science, 1(1), 7 (2017). https://doi.org/10.3390/jcs1010007

[42] Coppola B, Emilia G, Luciano DM. : Investigation on the use of PLA/hemp composites for the fused deposition modelling (FDM) 3D printing. AIP Conference Proceedings, 1981, 020086 (2018). https://doi.org/10.1063/1.5045948

[43] Sawpan MA, Pickering KL, Fernyhough A. : Effect of fibre treatments on interfacial shear strength of hemp fibre reinforced polylactide and unsaturated polyester composites. Composites Part A: Applied Science and Manufacturing, 42, 1189–1196 (2011). https://doi.org/10.1016/j.compositesa.2011.05.003

[44] Aliotta L, Cinelli P, Coltelli MB, Righetti MC, Gazzano M, Lazzeri A. : Effect of nucleating agents on crystallinity and properties of poly (lactic acid) (PLA). European Polymer Journal 93, 822–832 (2017). https://doi.org/10.1016/j.eurpolymj.2017.04.041.

[45] Dai JX, Yang Q, Liu BJ. : Crystallization Behavior of PLA/PEG/Nucleating Agent Blends. Advanced Materials Research, 807–809, 578–581 (2013). https://doi.org/10.4028/www.scientific.net/AMR.807-809.578

[46] Tang Z, Zhang C, Liu X, Zhu J. : The crystallization behavior and mechanical properties of polylactic acid in the presence of a crystal nucleating agent. Journal of Applied Polymer Science 125, 1108–1115 (2012). https://doi.org/10.1002/app.34799.

[47] Ahmad SM, Pickering K, Fernyhough A. : Characterisation of hemp fibre reinforced poly(lactic acid). International Journal of Materials and Product Technology 36, 229–240 (2009).

[48] Delphine D, Michiel B, Kevin H, Wim S, Eleonora F, Frederik D, Jan I, Aart WVV,. Production and characterization of bamboo and flax fiber reinforced polylactic acid filaments for fused deposition modeling (FDM). Polymer Composites, 40, 1951-1963 (2018). https://doi.org/10.1002/pc.24971.

[49] David S, Kim LP, Yuanji Z. : Fused Deposition Modelling of Natural Fibre/Polylactic Acid Composites, 1(1), 8 (2017). https://doi.org/10.3390/jcs1010008

[50] George J, Ishida H. : A review on the very high nanofiller-content nanocomposites: Their preparation methods and properties with high aspect ratio fillers. Progress in Polymer Science, 86, 1–39 (2018). https://doi.org/10.1016/j.progpolymsci.2018.07.006

[51] Moudood A, Rahman A, Öchsner A, Islam M, Francucci G. :. Flax fiber and its composites: An overview of water and moisture absorption impact on their performance. Journal of Reinforced Plastics and Composites, 38, 323–339 (2019). https://doi.org/10.1177/0731684418818893.

[52] Charles DK, Frédéric D, Adam P, Antoine LD, Fabrizio S. The Design of 4D-Printed Hygromorphs: State-of-the-Art and Future Challenges. Advanced Functional Materials, 33, 2210353 (2023). https://doi.org/10.1002/adfm.202210353

[53] Mohammed M, Jawad AJM, Mohammed AM, Oleiwi JK, Adam T, Osman AF, Dahham OS, Betar BO, Gopinath SCB, Jaafar M. : Challenges and advancement in water absorption of natural fiber-reinforced polymer composites. Polymer Testing, 124, 108083 (2023). https://doi.org/10.1016/j.polymertesting.2023.108083.

[54] Bi X, Huang R. : 3D printing of natural fiber and composites: A state-of-the-art review. Materials & Design, 222, 111065 (2022). https://doi.org/10.1016/j.matdes.2022.111065.

[55] Kim YJ, Hong SJ, Shin WS, Kwon YR, Lim SH, Kim JS, Choi J, Kim JW, Kim DH. : Preparation and Performance of Superabsorbent Polymer with Cellulose Additives. Fibers Polym 21, 2448–2455 (2020). https://doi.org/10.1007/s12221-020-1198-5.

[56] Lamm ME, Wang L, Kishore V, Tekinalp H, Kunc V, Wang J, Gardner DJ, Ozcan S. : Material Extrusion Additive Manufacturing of Wood and Lignocellulosic Filled Composites. Polymers 12, 2115 (2020). https://doi.org/10.3390/polym12092115.

[57] Rakesh P, Singh I. : Processing of Green Composites (2019). https://doi.org/10.1007/978-981-13-6019-0

[58] Yu N, Sun X, Wang Z, Zhang D, Li J. : Effects of auxiliary heat on the interlayer bonds and mechanical performance of polylactide manufactured through fused deposition modeling. Polymer Testing, 104, 107390 (2021). https://doi.org/10.1016/j.polymertesting.2021.107390

[59] Pokharel A, Falua KJ, Babaei GA, Acharya B. : Biobased Polymer Composites: A Review. Journal of Composites Science, 6(9), 255 (2022). https://doi.org/10.3390/jcs6090255.

[60] Bianchi I, Forcellese A, Gentili S, Greco L, Simoncini M. : Comparison between the mechanical properties and environmental impacts of 3D printed synthetic and bio-based composites. Procedia CIRP, 105, 380–5 (2022). https://doi.org/10.1016/j.procir.2022.02.063.

[61] Ilyas RA, Sapuan SM, Harussani MM, Hakimi MYAY, Haziq MZM, Atikah MSN. : Polylactic Acid (PLA) Biocomposite: Processing, Additive Manufacturing and Advanced Applications. Polymers, 13, 1326 (2021). https://doi.org/10.3390/polym13081326.

[62] Momeni S, Safder M, Khondoker MAH, Elias AL. : Valorization of Hemp Hurds as Bio-Sourced Additives in PLA-Based Biocomposites. Polymers, 13, 3786 (2021). https://doi.org/10.3390/polym13213786.

[63] Yang S, Ma K, Liu Z, Ren J, Man Y. : Chapter 5 - Development and applicability of life cycle impact assessment methodologies. Life Cycle Sustainability Assessment for Decision-Making, 95–124 (2020). https://doi.org/10.1016/B978-0-12-818355-7.00005-1

[64] Muralikrishna IV, Manickam V. : Chapter Five - Life Cycle Assessment. Environmental Management, 57–75 (2017). https://doi.org/10.1016/B978-0-12-811989-1.00005-1.

[65] Hervy M, Evangelisti S, Lettieri P, Lee KY. : Life cycle assessment of nanocellulose-reinforced advanced fibre composites. Composites Science and Technology, 118, 154–62 (2015). https://doi.org/10.1016/j.compscitech.2015.08.024.

[66] Kumar R, Sharma H, Saran C, Tripathy TS, Sangwan KS, Herrmann C. A Comparative Study on the Life Cycle Assessment of a 3D Printed Product with PLA, ABS & PETG Materials. Procedia CIRP, 107, 15–20 (2022). https://doi.org/10.1016/j.procir.2022.04.003.

[67] Enarevba DR, Haapala KR. A Comparative Life Cycle Assessment of Expanded Polystyrene and Mycelium Packaging Box Inserts. Procedia CIRP, 116, 654–9 (2023). https://doi.org/10.1016/j.procir.2023.02.110.

Dear Dr. Sadhan Jana,

Thank you very much for your kind letter. I greatly appreciate the editor and the reviewers for their positive and constructive comments and suggestions on our manuscript (PES-25-1682).

The authors have thoroughly considered all the comments of the reviewers and substantially revised the manuscript, and the revised parts are marked in red. A point-by-point response to the reviewer's comments is proposed to highlight the contribution of this research work and clarify its novelty. Some new discussions have been inserted in this manuscript to overcome the weakness indicated by the reviewers. I would like to resubmit the revised manuscript for your kind consideration. I believe the modifications will be satisfactory and the revised manuscript is suitable for publication in *Polymer Engineering & Science*.

Thank you and best regards.

Yours sincerely,

Dr. Faleh RABHI

faleh.rabhi@femto-st.fr

Rheological, mechanical and life cycle assessment of 3D-printed PLA/Hemp/PEG biocomposites

Manuscript ID: PES-25-1682

I greatly appreciate the editor's effort in handling the manuscript and the constructive comments from the reviewers. All the comments have been addressed to improve the quality of the revised manuscript. The detailed "**Response to the reviews**" and "**Summary of changes**" are presented below.

Response to the reviewers

Editorial changes required:

Questions:

Q1- We do not publish glossary. I ask that you define all the variables within the text.

Q2- Remove boxes from around the figures.

Q3- Present Figure 7 with white background.

Answers:

R1-2-3- Thank you for your constructive comments. The various requests have been made in the revised paper.

Reviewer: 1

Questions:

Q1- In section 2: Please replace 'Description of PLA" by "Properties of PLA"

"Properties of the PLA/Hemp/PEG composites".

Q2- Please specify the used nozzle diameter. If it is of 0.4mm (standard diameter), the layer thickness cannot exceed 0.4mm !!.

Q3- Please justify the choice of a raster angle of 45° and -45°.

Q4- Please provide the tensile stress-strain curves to identify the failure mode.

Q5- For the contribution analysis, indicate the material and not the manufacturing technique (replace 3D-printing by PLA/Hemp/PEG composites).

Answers:

R1- Thank you for your comments. The proposed title is used in the revised paper.

R2- Thank you for this relevant comment. The nozzle diameter is 1 mm. This value is already defined in original paper in sentence after table 5 in section 3.2.

R3- Thank you for your constructive comments. The answer to your question has been added to the body of the article (section 3.2 after Table 6).

R4- Thank you for this pertinent remark. The requested figure (figure 8) has been inserted in section 3.4 and the associated mechanical analyses have been inserted in the revised paper.

R5- Thank you for your comments. The requested changes and modifications have been made in the body of section 3.5 of the article.

Reviewer: 2

Questions:

Q1- While the paper is generally well-written, several aspects require further attention: Material formulation: the study focuses on a single formulation (20% hemp / 5% PEG), which appears to be a pre-existing industrial product. The choice of this specific composition needs stronger justification. Specifically, the authors should explain why the PEG content was not varied or optimized, given its critical role in modifying rheological behavior and printability.

Q2- DOE and porosity analysis: although a DOE approach was used to optimize working parameters (including temperature), the specific impact of each parameter on porosity is unclear. The analysis should better explicate how individual parameters and their combinations (interaction effects) influence the porosity of the printed samples.

Q3- In particular, the DOE section identifies optimal parameters, but the discussion on why these specific combinations work is limited. To consider adding interaction plots (e.g., Temperature vs. Flow Rate on Porosity) to visually demonstrate how these variables influence the final density would significantly strengthen the correlation between process parameters and material quality.

Answers:

R1- Thank you for your constructive comments. Some sentences have been added in

the revised paper to describe the optimal formulation of PLA/PEG/Hemp (section 2.1.2) in terms of printed components with no defect and best mechanical properties.

R2- Thank you for your comments. The answer to your question has been added in the revised paper (section 3.2, before Figure 5). No significant interactions were evident in main effects plots; interaction plots were thus not pursued, per standard Taguchi practice. Revised discussion clarifies this rationale.

R3- Thank you for your comments. The answer to your question has been added to the body of the article (section 3.2, after Table 5).

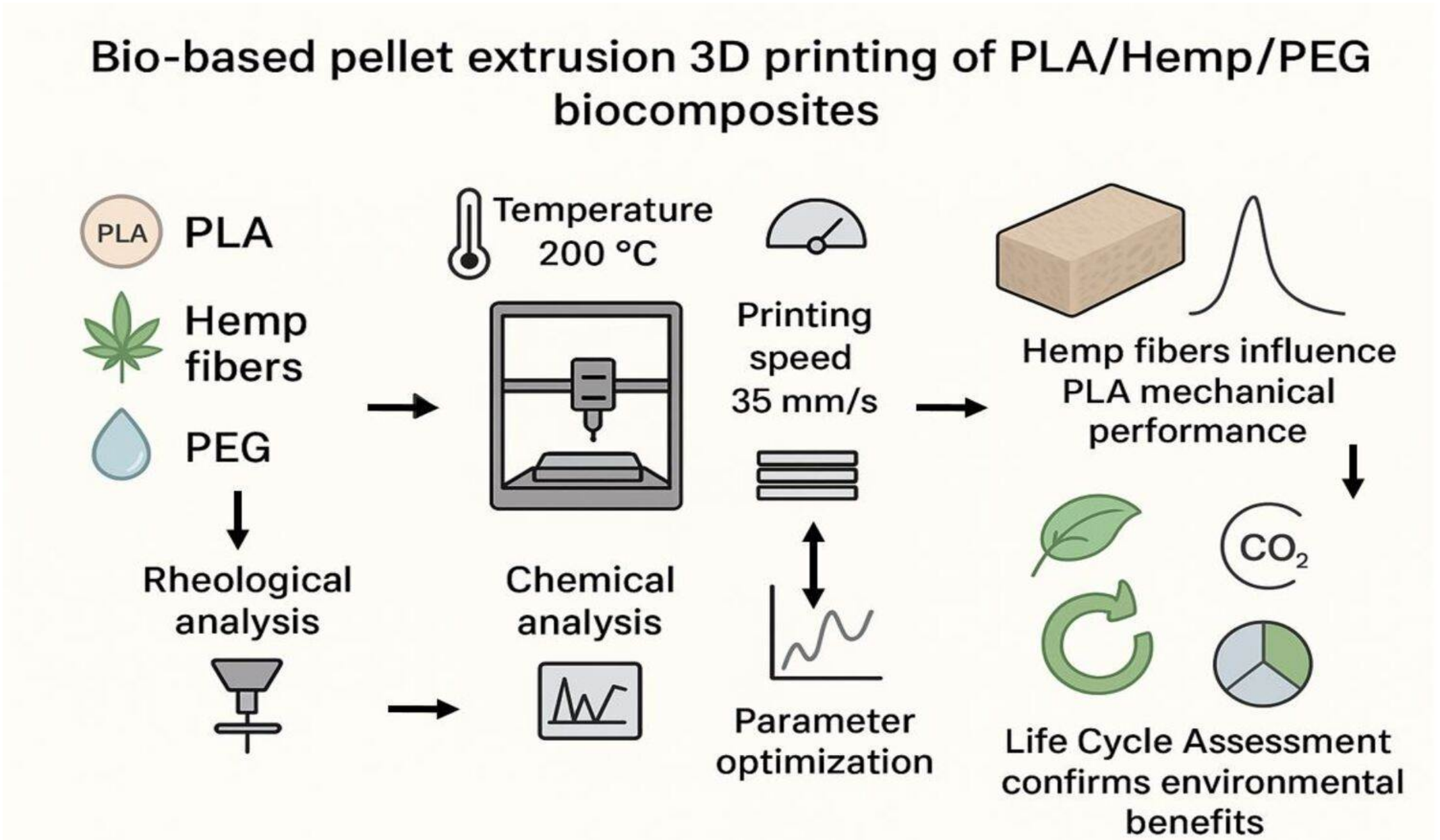
Bio-based pellet extrusion 3D printing of PLA/Hemp/PEG biocomposites
PLA
PLA
Hemp fibers
PEG
Rheological analysis
Temperature 200 °C
Chemical analysis
Printing speed 35 mm/s
Parameter optimization
Hemp fibers influence PLA mechanical performance
CO_2
Life Cycle Assessment confirms environmental benefits